Vif AND Vpu PROTEINS

Vif protein is essential for viral replication in natural target cells such as CD4-positve lymphocytes and macrophages. Recent identification of its cellular object for attack (Sheehy et al., 2002) has clearly revealed the biological and biochemical bases for the growth property of ΔVif virus in natural target cells. This finding (identification of a family of APOBEC3 proteins, cellular cytidine deaminases, as potent inhibitors of HIV-1 replication in primary cells) has also contributed much to establish the concept of "the restriction factor" to well understand virus–cell interaction (Malim and Emerman, 2008; Sato et al., 2012). Of the APOBEC3 family proteins, APOBEC3G and APOBEC3F (Kitamura et al., 2011) strongly inhibit viral replication in the absence of Vif (**Figure 3**). Although HIV-1 Vif can abrogate the activities of human APOBEC3, it cannot do so against monkey APOBEC3. In contrast, SIVmac Vif can neutralize the antiviral activity of APOBEC3 of both origins. Finally, it has been demonstrated that Vif and APOBEC3 are the major determinants for the HIV-1 species tropism by constructing macaque-tropic HIV-1 (HIV-1mt) and monitoring the HIV-1mt growth property in various genetic contexts of macaques (Hatziioannou et al., 2006, 2009; Kamada et al., 2006; Igarashi et al., 2007; Thippeshappa et al., 2011).

Vpu protein, unique to viruses of the HIV-1 group (**Figure 1**), modulates viral replication in human CD4-positive cell lines and primary cells. Mutant HIV-1 without Vpu (ΔVpu virus) grows poorly relative to wild-type virus. Recently, a cellular protein named Tetherin (also called BST-2) has been identified as a restriction factor against HIV-1 and is antagonized by Vpu (Neil et al., 2008; Van Damme et al., 2008). Vpu down-regulates the Tetherin from cell surface, and thereby promotes extracellular production of progeny virions (Malim and Emerman, 2008; Arias et al., 2011; Sato et al., 2012). The baseline mechanism for this action of Vpu is well studied as shown in **Figure 4**. Here, it must be attentive that the anti-Tetherin activity of Vpu is host species-specific as observed for Vif. HIV-1 Vpu acts against human but not (or poorly) macaque Tetherins (Sauter et al., 2009, 2010). Although the biological effect of Vpu is much milder than that of Vif as judged by the growth kinetics of mutant viruses (**Figure 2**), Vpu may be critical for interspecies transmission

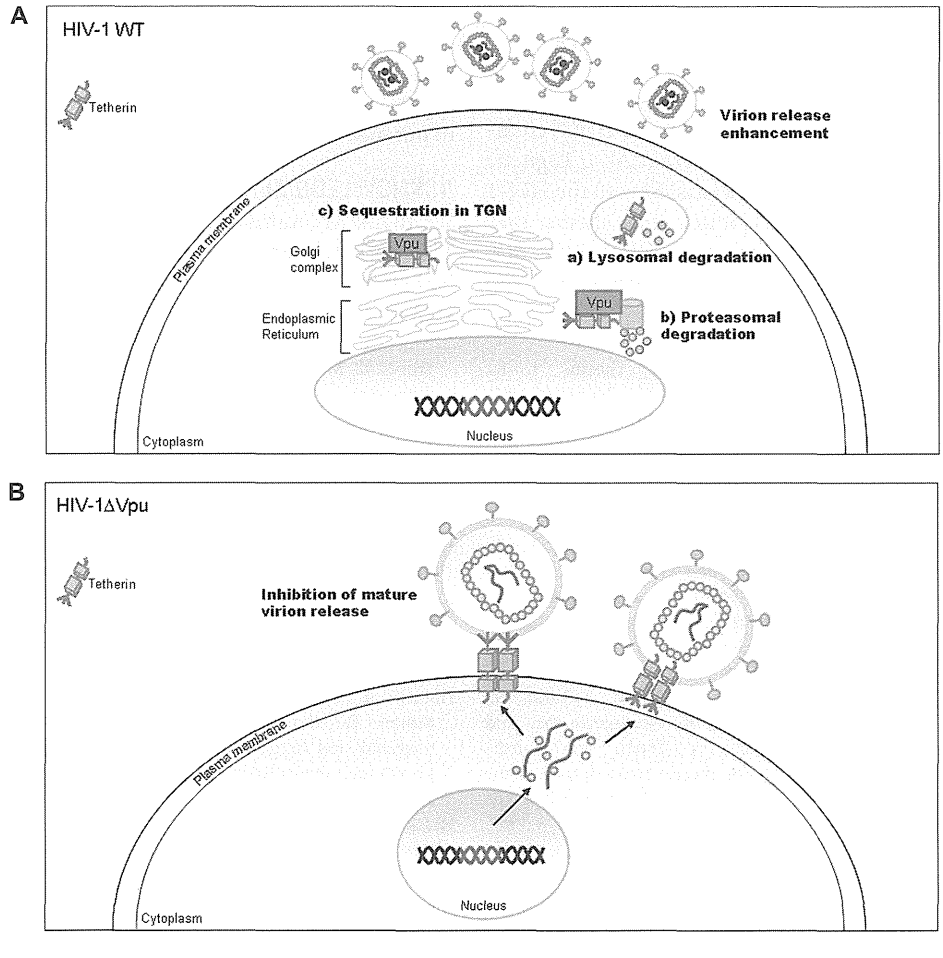

FIGURE 4 | HIV-1 replication and Tetherin. On the basis of results reported so far, the action mechanism of Vpu is depicted. Replication process for wild-type (WT) and ΔVpu mutant viruses are schematically shown on the basis of previously reported review articles (Tokarev et al., 2009; Douglas et al., 2010; Evans et al., 2010). TGN, trans-Golgi network.

through mutation/adaptation/recombinations (Kirchhoff, 2009; Sauter et al., 2009, 2010; Sharp and Hahn, 2011). Thus, Vpu and Tetherin affect the HIV-1 species tropism, but the effect may be relatively small.

In sum, Vif and Vpu counteract the major restriction factors APOBEC3 proteins and Tetherin/BST-2, respectively, and represent viral determinants for the host range of HIV-1 (**Tables 1 and 2**). It is intriguing to note that these factors would have shaped HIV-1 and made it unique among various primate immunodeficiency viruses (**Figure 1**).

Vpx AND Vpr PROTEINS

Vpx and Vpr proteins are necessary for efficient viral replication (Malim and Emerman, 2008; Fujita et al., 2010). In macrophages, ΔVpx replication is not detectable and this defect has been shown to be present at post-entry and before/during the reverse transcription process (Fujita et al., 2008, 2010; Srivastava et al., 2008). Also in some lymphocyte cell lines and in primary lymphocytes, Vpx protein is critical for viral replication (Ueno et al., 2003; Fujita et al., 2010; Doi et al., 2011). Because ΔVpr virus is somewhat replication-defective in some cells (for both HIV-1 and HIV-2), it is not unreasonable to assume that Vpr may play a role in the viral growth cycle. As such, Vpx and Vpr are important for *in vivo* viral replication and finally for viral pathogenicity (Fujita et al., 2010).

Very recently, SAMHD1 and APOBEC3A have been reported to be myeloid cell-specific restriction factors against HIV-1 counteracted by Vpx (Berger et al., 2011; Hrecka et al., 2011; Laguette et al., 2011). Whether these proteins are associated with the HIV-1 species tropism described in this review article, and whether they can explain the *in vitro* and *in vivo* situation of HIV-2/SIVmac mutant viruses mentioned above remain to be determined (Fujita et al., 2010; Nomaguchi et al., 2011).

CONCLUSION

In this review, we have described the major determinants for the species tropism of HIV-1. Structural Gag-CA and accessory Vif and Vpu proteins are clearly involved in this host range of HIV-1 as viral factors (**Table 1**). Cellular proteins that interact with these and contribute to this tropism are definitely the restriction factors (**Table 1**). In total, interplays between the viral and cellular responsible factors decide this unique and limited tropism of HIV-1. Whether there are the other factors that affect the HIV-1 species tropism is awaiting further investigations. In this regard, the biology of Vpx deserves attention. Because Vpx is present in SIVmac but not in HIV-1 (**Figure 1**), it may inactivate a cellular anti-viral protein(s) which is not recognized by HIV-1 proteins.

In both basic and applicable points of view, the narrow host range of HIV-1 is burdensome obstacle to overcome. Assuming that HIV-1mt can grow and cause disease similarly with SIVmac in macaques, we would be able to better perform model studies to precisely analyze viral replication and pathogenicity *in vivo*, and to establish the effective anti-HIV-1/AIDS strategies. To the best of our knowledge, there are no such HIV-1mt clones so far (Hatziioannou et al., 2006, 2009; Kamada et al., 2006; Igarashi et al., 2007; Kuroishi et al., 2009; Saito et al., 2011; Thippeshappa et al., 2011). We may further improve the ability of HIV-1mt by today's powerful methodology if we knew all the cellular determinants for the species tropism of HIV-1. Studies in this direction are in progress in our laboratory.

ACKNOWLEDGMENTS

We thank Ms Kazuko Yoshida for excellent editorial assistance. This work was supported by a grant from the Ministry of Health, Labour and Welfare of Japan (Research on HIV/AIDS project no. H22-003).

REFERENCES

Arias, J. F., Iwabu, Y., and Tokunaga, K. (2011). Structural basis for the antiviral activity of BST-2/tetherin and its viral antagonism. *Front. Microbiol.* 2:250. doi: 10.3389/fmicb.2011.00250

Berger, G., Durand S., Fargier, G., Nguyen, X.-N., Cordeil, S., Bouaziz, S., Muriaux, D., Darlix, J.-L., and Cimarelli, A. (2011). APOBEC3A is a specific inhibitor of the early phases of HIV-1 infection in myeloid cells. *PLoS Pathog.* 7, e1002221. doi: 10.1371/journal.ppat.1002221

Doi, N., Fujiwara, S., Adachi, A., and Nomaguchi, M. (2011). Rhesus M1.3S cells suitable for biological evaluation of macaque-tropic HIV/SIV clones. *Front. Microbiol.* 2:115. doi: 10.3389/fmicb.2011.00115

Dorfman, T., and Gottlinger, H. G. (1996). The human immunodeficiency virus type 1 capsid p2 domain confers sensitivity to the cyclophilin-binding drug SDZ NIM 811. *J. Virol.* 70, 5751–5757.

Douglas, J. L., Gustin, J. K., Viswanathan, K., Mansouri, M., Moses, A. V., and Fruh, K. (2010). The great escape: viral strategies to counter BST-2/tetherin. *PLoS Pathog.* 6, e1000913. doi: 10.1371/journal.ppat.1000913

Evans, D. T., Serra-Moreno, R., Singh, R. K., and Guatelli, J. C. (2010). BST-2/tetherin: a new component of the innate immune response to enveloped viruses. *Trends Microbiol.* 18, 388–396.

Fujita, M., Otsuka, M., Miyoshi, M., Khamsri, B., Nomaguchi, M., and Adachi, A. (2008). Vpx is critical for reverse transcription of the human immunodeficiency virus type 2 genome in macrophages. *J. Virol.* 82, 7752–7756.

Fujita, M., Otsuka, M., Nomaguchi, M., and Adachi, A. (2010). Multifaceted activity of HIV Vpr/Vpx proteins: the current view of their virological functions. *Rev. Med. Virol.* 20, 68–76.

Hatziioannou, T., Ambrose, Z., Chung, N. P. Y., Piatak, M. Jr., Yuan, F., Trubey, C. M., Coalter, V., Kiser, R., Schneider, D., Smedley, J., Pung, R., Gathuka, M., Estes, J. D., Veazey, R. S., KewalRamani, V. N., Lifson, J. D., and Bieniasz, P. D. (2009). A macaque model of HIV-1 infection. *Proc. Natl. Acad. Sci. U.S.A.* 106, 4425–4429.

Hatziioannou, T., Princiotta, M., Piatak, M. Jr., Yuan, F., Zhang, F., Lifson, J. D., and Bieniasz, P. D. (2006). Generation of siman-tropic HIV-1 by restriction factor evasion. *Science* 314, 95.

Holmes, R. K., Malim, M. H., and Bishop, K. N. (2007). APOBEC-mediated viral restriction: not simply editing? *Trends Biochem. Sci.* 32, 118–128.

Hrecka, K., Hao, C., Gierszewska, M., Swanson, S. K., Kesik-Brodacka, M., Srivastava, S., Florens, L., Washburn, M. P., and Skowronski, J. (2011). Vpx relieves inhibition of HIV-1 infection of macrophages mediated by the SAMHD1 protein. *Nature* 474, 658–661.

Huthoff, H., and Towers, G. J. (2008). Restriction of retroviral replication by APOBEC3G/F and TRIM5alpha. *Trends Microbiol.* 16, 612–619.

Igarashi, T., Iyengar, R., Byrum, R. A., Buckler-White, A., Dewar, R. L., Buckler, C. E., Lane, H. C., Kamada, K., Adachi, A., and Martin, M. A. (2007). Human immunodeficiency virus type 1 derivative with 7% simian immunodeficiency virus genetic content is able to establish infections in pig-tailed macaques. *J. Virol.* 81, 11549–11552.

Kamada, K., Igarashi, T., Martin, M. A., Khamsri, B., Hatcho, K., Yamashita, T., Fujita, M., Uchiyama, T., and Adachi, A. (2006). Generation of HIV-1 derivatives that productively infect macaque monkey lymphoid cells. *Proc. Natl. Acad. Sci. U.S.A.*103, 16959–16964.

Khamsri, B., Murao, F., Yoshida, A., Sakurai, A., Uchiyama, T., Shirai, H., Matsuo, Y., Fujita, M., and Adachi, A. (2006). Comparative study on the structure and cytopathogenic activity of HIV Vpx/Vpr proteins. *Microbes Infect.* 8, 10–15.

Kirchhoff, F. (2009). Is the high virulence of HIV-1 an unfortunate coincidence of primate lentiviral evolution? *Nat. Rev. Microbiol.* 7, 467–476.

Kitamura, S., Ode, H., and Iwatani, Y. (2011). Structual features of antiviral APOBEC3 proteins are linked to their functional activities. *Front. Microbiol.* 2:258. doi: 10.3889/fmicb.2011.00258

Kuroishi, A., Saito, A., Shingai, Y., Shioda, T., Nomaguchi, M., Adachi, A., Akari, H., and Nakayama, E. E. (2009). Modification of a loop sequensce between alpha-helices 6 and 7 of virus capsid (CA) protein in a human immunodeficiency virus type 1 (HIV-1) derivative that has simian immunodeficiency virus (SIVmac239) Vif and CA alpha-helices 4 and 5 loop improves replication in cynomolgus monkey cells. *Retrovirology* 6, 70.

Laguette, N., Sobhian, B., Casartelli, N., Ringeard, M., Chable-Bessia, C., Segeral, E., Yatim, A., Emiliani, S., Schwartz, O., and Benkirane, M. (2011). SAMHD1 is the dendritic- and myeloid-cell-specific HIV-1 restriction factor counteracted by Vpx. *Nature* 474, 654–657.

Malim, M. H., and Emerman, M. (2008). HIV-1 accessory proteins-ensuring viral survival in a hostile environment. *Cell Host Microbe* 3, 388–398.

Nakayama, E. E., and Shioda, T. (2012). TRIM5α and species tropism of HIV/SIV. *Front. Microbiol.* 3:13. doi: 10.3389/fmicb.2012.00013

Neil, S. J., Zang, T., and Bieniasz, P. D. (2008). Tether ininhibits retrovirus release and is antagonized by HIV-1 Vpu. *Nature* 451, 425–430.

Nomaguchi, M., Doi, N., Kamada, K., and Adachi, A. (2008). Species barrier of HIV-1 and its jumping by virus engineering. *Rev. Med. Virol.* 18, 261–275.

Nomaguchi, M., Fujita, M., and Adachi, A. (2011). The fourth major restriction factor against HIV/SIV. *Front. Microbiol.* 2:132. doi: 10.3389/fmicb.2011.00132

Saito, A., Nomaguchi, M., Iijima, S., Kuroishi, A., Yoshida, T., Lee, Y. J., Hayakawa, T., Kono, K., Nakayama, E. E., Shioda, T., Yasutomi, Y., Adachi, A., Matano, T., and Akari, H. (2011). Improved capacity of a monkey-tropic HIV-1 derivative to replicate in cynomolgus monkeys with minimal modifications. *Microbes Infect.* 13, 58–64.

Sakuma, R., and Takeuchi, H. (2012). SIV replication in human cells. *Front. Microbiol.* 3:162. doi: 10.3389/fmicb.2012.00162

Sato, K., Gee, P., and Koyanagi, Y. (2012). Vpu and BST-2: still not there yet? *Front. Microbiol.* 3:131. doi: 10.3389/fmicb.2012.00131

Sauter, D., Schindler, M., Specht, A., Landford, W. N., Munch, J., Kim, K.-A., Votteler, J., Schubert, U., Bibollet-Ruche, F., Keele, B. R. F., Takehisa, J., Ogando, Y., Ochsenbauer, C., Kappes, J. C., Ayouba, A., Peeters, M., Learn, G. H., Shaw, G., Sharp, P. M., Bieniasz, P., Hahn, B. H., Hatzioannou, T., and Kirchhoff, F. (2009). Tetherin-driven adaptation of Vpu and Nef function and the evolution of pandemic and nonpandemic HIV-1 strains. *Cell Host Microbe* 6, 409–421.

Sauter, D., Specht, A., and Kirchhoff, F. (2010). Tetherin: holding on and letting go. *Cell* 141, 392–398.

Sharp, P. M., and Hahn, B. H. (2011). Origins of HIV and the AIDS pandemic. *Cold Spring Harb. Perspect. Med.* 1, a006841.

Sheehy, A. M., Gaddis, N. C., Choi, J. D., and Malim, M. H. (2002). Isolation of a human gene that inhibits HIV-1 infection and is suppressed by the viral Vif protein. *Nature* 418, 646–650.

Shibata, R., and Adachi, A. (1992). SIV/HIV recombinants and their use in studying biological properties. *AIDS Res. Hum. Retroviruses* 8, 403–409.

Shibata, R., Kawamura, M., Sakai, H., Hayami, M., Ishimoto, A., and Adachi, A. (1991). Generation of a chimeric human and simian immunodeficiency virus infectious to monkey peripheral blood mononuclear cells. *J. Virol.* 65, 3514–3520.

Shibata, R., Sakai, H., Kawamura, M., Tokunaga, K., and Adachi, A. (1995). Early replication block of human immunodeficiency type 1 in monkey cells. *J. Gen. Virol.* 76, 2723–2730.

Srivastava, S., Swanson, S. K., Manel, N., Florens, L., Washburn, M. P., and Skowronski, J. (2008). Lentiviral Vpx accessory factor targets VprBP/DCAF1 substrate adaptor for cullin 4 E3 ubiquitin ligase to enable to enhance macrophage infection. *PLoS Pathog.* 4, e1000059. doi: 10.1371/journal.ppat.1000059

Strebel, K., Luban, J., and Jeang, K. T. (2009). Human cellular restriction factors that target HIV-1 replication. *BMC Med.* 7, 48. doi: 10.1186/1741-7015-7-48

Thippeshappa, R., Polacino, P., Kimata, M. T. Y., Siwak, E. B., Anderson, D., Wang, W., Sherwood, L., Arora, R., Wen, M., Zhou, P., Hu, S.-L., and Kimata, J. T. (2011). Vif substitution enables persistent infection of pig-tailed macaques by human immunodeficiency virus type 1. *J. Virol.* 85, 3767–3779.

Tokarev, A., Skasko, M., Fitzpatrick, K., and Guatelli, J. (2009). Antiviral activity of the interferon-induced cellular protein BST-2/tetherin. *AIDS Res. Hum. Retroviruses* 25, 1197–1210.

Ueno, F., Shiota, H., Miyaura, M., Yoshida, A., Sakurai, A., Tatsuki, J., Koyama, A. H., Akari, H., Adachi, A., and Fujita, M. (2003). Vpx and Vpr proteins up-regulate the viral infectivity by a distinct mechanism in lymphocytic cells. *Microbes Infect.* 5, 387–395.

Van Damme, N., Goff, D., Katsura, C., Jorgenson, R. L., Mitchell, R., Johnson, M. C., Stephens, E. B., and Guatelli, J. (2008). The interferon-induced protein BST-2 restricts HIV-1 release and is down-regulated from the cell surface by the Vpu protein. *Cell Host Microbe* 3, 245–252.

Conflict of Interest Statement: The authors declare that the research was conducted in the absence of any commercial or financial relationships that could be construed as a potential conflict of interest.

Received: 02 July 2012; paper pending published: 08 July 2012; accepted: 09 July 2012; published online: 26 July 2012.

Citation: Nomaguchi M, Doi N, Matsumoto Y, Sakai Y, Fujiwara S and Adachi A (2012) Species tropism of HIV-1 modulated by viral accessory proteins. Front. Microbio. 3:267. doi: 10.3389/fmicb.2012.00267

This article was submitted to Frontiers in Virology, a specialty of Frontiers in Microbiology.

The Journal of Immunology

The Endothelial Antigen ESAM Monitors Hematopoietic Stem Cell Status between Quiescence and Self-Renewal

Takao Sudo,* Takafumi Yokota,* Kenji Oritani,* Yusuke Satoh,* Tatsuki Sugiyama,† Tatsuro Ishida,‡ Hirohiko Shibayama,* Sachiko Ezoe,* Natsuko Fujita,* Hirokazu Tanaka,*,[1] Tetsuo Maeda,* Takashi Nagasawa,† and Yuzuru Kanakura*

Whereas most hematopoietic stem cells (HSC) are quiescent in homeostasis, they actively proliferate in response to bone marrow (BM) injury. Signals from the BM microenvironment are thought to promote entry of HSC into the cell cycle. However, it has been cumbersome to assess cycle status of viable HSC and thus explore unique features associated with division. In this study, we show that expression of endothelial cell-selective adhesion molecule (ESAM) can be a powerful indicator of HSC activation. ESAM levels clearly mirrored the shift of HSC between quiescence and activation, and it was prominent in comparison with other HSC-related Ags. ESAM^{hi} HSC were actively dividing, but had surprisingly high long-term reconstituting capacity. Immunohistochemical analyses showed that most ESAM^{hi} HSC were located near vascular endothelium in the BM after 5-fluorouracil treatment. To determine the importance of ESAM in the process of BM recovery, ESAM knockout mice were treated with 5-fluorouracil and their hematopoietic reconstruction was examined. The ESAM deficiency caused severe and prolonged BM suppression, suggesting that ESAM is functionally indispensable for HSC to re-establish homeostatic hematopoiesis. With respect to intracellular regulators, NF-κB and topoisomerase II levels correlated with the ESAM upregulation. Thus, our data demonstrate that the intensity of ESAM expression is useful to trace activated HSC and to understand molecular events involved in stem cell states. ***The Journal of Immunology*****, 2012, 189: 200–210.**

Hematopoietic stem cells (HSC) are characterized as being extensively self-renewing as well as multipotent. Distinction of HSC from differentiating cells is essential for understanding the essence of "stemness." Many groups have identified HSC-related Ags, and those markers have made it possible to sort long-term reconstituting HSC (LT-HSC) with high purity. For example, at least one in three lineage (Lin)$^-$c-Kit^{hi}Sca-1$^+$CD34$^-$Flk2/Flt3$^-$CD150$^+$CD48$^-$ fraction cells in adult mouse bone marrow (BM) can be transplanted (1–3). Recent studies using a BrdU-retaining method and/or a histone 2B-GFP transgene have shown that the long-term reconstituting activity of the adult mouse BM is sustained mostly in very quiescent HSC that divide only five to six times during the adult period (4, 5). However, even the highly purified LT-HSC fraction is heterogeneous with respect to cell cycle status (4, 5).

The cell cycle status and differentiating behavior of HSC are known to fluctuate according to physiological circumstances. During fetal and early postnatal periods, development of the hematopoietic system is essential in supporting the rapid growth of organisms and the explosive expansion of all blood lineages. Indeed, numbers of HSC increase ~40-fold in the fetal liver between embryonic days 12 and 16 (6). Alternatively, upon reaching adulthood, HSC become quiescent and evade exhaustion or mutation to maintain hematopoiesis throughout life (7). Although the quiescent HSC divide at an extremely low rate during homeostasis, they are rapidly activated to proliferate in response to BM injury or by G-CSF stimulation (5). Interestingly, after re-establishment of homeostasis, the activated HSC can return to quiescence. Distinguishing LT-HSC from differentiating progenitors becomes complicated by BM injury because the expression pattern of HSC-related Ags is dramatically influenced (8). Molecular crosstalk between HSC and the BM microenvironment, also known as "HSC niche," is likely to control the balance of HSC quiescence and activity (9, 10), but precise mechanisms regulating HSC status remain largely unknown. If we could selectively isolate active HSC with a set of surface markers, that should yield significant insights regarding HSC biology and HSC applications for clinical purposes. Furthermore, information about cell surface Ags that mirror HSC states would be invaluable for understanding the relationship between HSC and their niches.

Endothelial cell-selective adhesion molecule (ESAM), which is an Ig superfamily protein, was originally identified as an endothelial specific molecule mediating cell–cell adhesion through homophilic interactions (11, 12). ESAM proteins colocalize with cadherins and catenins in cell–cell junctions of vascular endothelium. ESAM deficiency in endothelial tight junctions disturbs neutrophil extravasation to inflamed tissues by reduction of acti-

*Department of Hematology and Oncology, Osaka University Graduate School of Medicine, Suita, Osaka 565-0871, Japan; †Department of Immunobiology and Hematology, Institute for Frontier Medical Sciences, Kyoto University, Kyoto 606-8507, Japan; and ‡Division of Cardiovascular Medicine, Department of Internal Medicine, Kobe University Graduate School of Medicine, Kobe, Hyogo 650-0017, Japan

[1]Current address: Division of Hematology, Department of Internal Medicine, Kinki University School of Medicine, Osaka, Japan.

Received for publication January 6, 2012. Accepted for publication May 2, 2012.

This work was supported in part by a grant from the Mitsubishi Pharma Research Foundation.

Address correspondence and reprint requests to Dr. Takafumi Yokota, Department of Hematology and Oncology, Osaka University Graduate School of Medicine, C9, 2-2 Yamadaoka, Suita, Osaka 565-0871, Japan. E-mail address: yokotat@bldon.med.osaka-u.ac.jp

The online version of this article contains supplemental material.

Abbreviations used in this article: BM, bone marrow; E, embryonic day; ESAM, endothelial cell-selective adhesion molecule; 5-FU, 5-fluorouracil; HSC, hematopoietic stem cell; KO, knockout; Lin, lineage; LSK, Lin$^-$Sca1$^+$c-Kit$^+$; LT-HSC, long-term reconstituting hematopoietic stem cell; ROS, reactive oxygen species; RU, repopulating unit; SAv, streptavidin; TR, Texas Red; WT, wild-type.

www.jimmunol.org/cgi/doi/10.4049/jimmunol.1200056

vated Rho proteins (13). The deficiency also increases vascular permeability of the renal glomeruli, resulting in urinary albumin elevation (14). Additionally, it has been shown that ESAM is also expressed on megakaryocytes and platelets (12), where it is involved in the regulation of thrombus formation (15).

Our recent study revealed that ESAM is also useful as an HSC marker (16). Hematopoietic and endothelial cells are both derived from mesoderm and share many features with respect to cell surface molecules. Some endothelial-related markers are known to become undetectable on HSC in adult BM, but they are upregulated upon hematopoietic reconstruction after treatment with myelosuppressive drugs or irradiation (17). Although ESAM marks LT-HSC throughout adult life, we observed that there are some age-related changes regarding the intensity of expression (16). We have now studied changes in ESAM levels on adult HSC following BM stress. Our data show that ESAM represents a powerful tool for monitoring the fluctuation between quiescence and self-renewal of the adult BM HSC. Additionally, our experiments using ESAM knockout (KO) mice suggest that ESAM is indispensable for normal hematopoietic recovery after BM injury.

Materials and Methods

Mice

Wild-type (WT) C57BL/6, BALB/c, and FVB mice were obtained from CLEA Japan (Shizuoka, Japan). The congenic C57BL/6 strain (C57BL/6SJL; CD45.1 alloantigen) was purchased from The Jackson Laboratory (Bar Harbor, ME) and used for transplantation experiments. ESAM KO mice were developed by Dr. T. Ishida (Kobe University, Kobe, Japan) as previously reported (18). Mating of heterozygous male and female mice was routinely performed to generate homozygous ESAM KO mice. Three types of PCR primers were used to genotype ESAM KO mice as documented previously (19). All mice used in this article were 8–12 wk old. Animal studies were performed with the approval of the Institutional Review Board of Osaka University.

Abs and reagents

5-Fluorouracil (5-FU) was purchased from Kyowa-Hakko Kirin (Tokyo, Japan). Purified anti-Ly6G and Ly6C/Gr1 (RB6-8C5) mAb, PE-conjugated anti-CD3e (145-2C11), CD45.1 (A20), and CD48 (HM48-1) mAbs, FITC-conjugated and allophycocyanin-conjugated anti-CD11b/Mac1 (M1/70), Ly6G and Ly6C/Gr1 (RB6-8C5), CD45R/B220 (RA3-6B2), Ter119, CD3e (145-2C11), and CD8a (53-6.7) mAbs, allophycocyanin-conjugated anti-CD117/c-Kit (2B8) mAb, PE-Cy7–conjugated anti-Sca1 (Ly6A/E; D7) mAb, biotinylated anti-Sca1 (E13-161.7) mAb, PerCP-Cy5.5–conjugated anti-CD45.2 (104) mAb, and Alexa Fluor 647-conjugated anti-CD19 (1D3) mAb, streptavidin (SAv)-PE, and SAv-PE-Texas Red (TR) were purchased from BD Pharmingen (San Diego, CA). Purified anti-CD3 (17A2), Mac1 (M1/70), and Ter119 mAbs, and PE-conjugated anti-CD105/endoglin (MJ7/18), CD31/PECAM-1 (390), Tie2 (TEK4), and CD135/Flt3 (A2F10) mAbs were purchased from eBioscience (San Diego, CA). PE-conjugated and allophycocyanin-conjugated anti-CD150 (TC15-12F12.2) mAbs and PerCP-Cy5.5–conjugated anti–CD117/c-Kit (2B8) mAb were purchased from BioLegend (San Diego, CA). Cy3-conjugated goat anti-rat IgG Ab was purchased from Jackson ImmunoResearch Laboratories (West Grove, PA). Streptavidin-Alexa Fluor 647 was purchased from Invitrogen (Carlsbad, CA). FITC-conjugated Ki67 (M-19) mAb was purchased from Santa Cruz Biotechnology (Santa Cruz, CA). A rat anti-mouse ESAM (1G8) mAb, which was originally developed and supplied by Drs. S. Butz and D. Vestweber (Max Planck Institute, Muenster, Germany), was purchased from BioLegend. The Ab was biotinylated in our hands using Sulfo-NHS-LC-Biotin (Thermo Fisher Scientific, Rockford, IL). Bortezomib (Velcade) was purchased from Janssen (Tokyo, Japan). ICRF-193 was purchased from Funakoshi (Tokyo, Japan). TaqMan FAM dye-labeled MGB probe sets for ESAM and GAPDH were purchased from Applied Biosystems (Foster City, CA).

Flow cytometry

Cells were obtained from adult mouse tissues indicated in each experiment and first incubated with a rat anti-mouse FcRII/III Ab (2.4G2) to block nonspecific Ab binding via FcR. Then, the cells were stained with the indicated Abs. Lin Abs contain anti-Mac1, Gr1, CD3e, CD45R/B220, and Ter119 Abs for analysis of untreated control mice, and Gr1, CD3e, CD45R/B220, and Ter119 for 5-FU–treated mice, as the level of Mac1 on HSC revives after a 5-FU treatment. A biotinylated anti-ESAM Ab was developed with SAv-PE or SAv-PE-TR. Flow cytometry analyses were performed with FACSAria or FACSCanto (BD Biosciences). The data analyses were done with FlowJo software (Tree Star, San Carlos, CA).

Quantitative real-time PCR

RNA samples from $Lin^-Sca1^+c\text{-}Kit^+$ (LSK) cells were isolated using a PureLink RNA Mini kit (Invitrogen). Reverse transcription reactions were performed using a high-capacity RNA-to-cDNA kit (Applied Biosystems). Relative expression levels of ESAM were evaluated according to TaqMan gene expression assay protocol (Applied Biosystems). Taqman FAM dye-labeled MGB probe sets for ESAM and GAPDH were purchased from Applied Biosystems. Reactions were run on the 7900HT Fast real-time PCR system (Applied Biosystems). The data were analyzed using SDS 2.3 software (Applied Biosystems).

Cell cycle analyses

Mice were given a single 5-FU injection and analyzed. BrdU was i.p. administered 12 h before analyses. BM cells were stained with biotynilated anti-ESAM, PE-Cy7-anti-Sca1, and allophycocyanin-anti–c-Kit Abs, followed by SAv-PE. The stained cells were then fixed, permeabilized, and incubated with DNase to expose incorporated BrdU by using a BrdU flow kit (BD Pharmingen). Subsequently, the cells were stained with FITC-anti-BrdU Ab for 30 min at room temperature and resuspended with staining medium containing 7-aminoactinomycin D. For another staining set, the cells were incubated with 2 μg/ml Hoechst 33342 (Sigma-Aldrich, St. Louis, MO) and FITC-anti-Ki67 Ab for 30 min at room temperature. Cell cycle statuses were analyzed by FACSAria (BD Biosciences).

Cell isolation

BM cells obtained from femora and tibiae of adult mice were first incubated with purified anti-Lin Abs, followed by goat anti-rat IgG microbeads (Miltenyi Biotec). After Lin^+ cell depletion, the Lin^--enriched cells were stained with FITC-anti-Lin Abs in combination with PE-Cy7-anti-Sca1, allophycocyanin-anti–c-Kit, and biotinylated anti-ESAM Abs. Subsequent to staining with SAv-PE, $ESAM^{lo}$ and $ESAM^{hi}$ LSK cells were sorted with FACSAria. The purity of the sorted cells was routinely confirmed by using a part of each sorted population to be >97%.

Methylcellulose cultures

C57BL/6 mice were treated with single i.v. 5-FU (150 mg/kg). Five days after treatment, mice were killed and $ESAM^{lo}$ or $ESAM^{hi}$ LSK cells of BM were sorted and subjected to methylcellulose colony formation assays. Two hundred cells of each sorted fraction were cultured in IMDM-based methylcellulose medium supplemented with 50 ng/ml recombinant murine stem cell factor, 10 ng/ml recombinant murine IL-3, 10 ng/ml recombinant human IL-6, and 3 U /ml recombinant human erythropoietin (Methocult GF 3434; StemCell Technologies, Vancouver, BC, Canada). After 9–10 d, colonies were enumerated and classified as CFU-GM, CFU-M, BFU-E, or CFU-Mix according to shape and color under an inverted microscope.

Competitive repopulation assay

Ly5 congenic mice were used for competitive repopulation assays. Two thousand $ESAM^{lo}$ LSK or $ESAM^{hi}$ LSK cells sorted from C57BL/6-Ly5.1 (CD45.1) mice were mixed with 2×10^5 unfractionated adult BM cells obtained from WT C57BL/6-Ly5.2 (CD45.2) mice and were transplanted into C57BL/6-Ly5.2 mice irradiated at a dose of 8.5 Gy. Peripheral blood analyses were performed at 4-wk intervals after transplantation. Sixteen weeks after transplantation, all recipients were killed and BM cells were collected. BM cells were stained with FITC-anti-Mac1, PE-anti-CD3e, Alexa Fluor 647-anti-CD19, PerCP-Cy5.5-anti-CD45.2, and PE-Cy7-anti-CD45.1 Abs to analyze the donor-derived chimerism and each lineage differentiation, and they were simultaneously stained with FITC-anti-Lin, PE-anti-CD45.1, PerCP-Cy5.5-anti-CD45.2, PE-Cy7-anti-Sca1, and allophycocyanin-anti–c-Kit, and biotinylated anti-ESAM Abs, followed by SAv-PE-TR to evaluate ESAM level of LSK fraction. The repopulating unit (RU) was calculated as follows: RU = [(% donor-derived cells) × (number of competitor cells/10^5)]/(% competitor-derived cells) (20). The total number of RU per BM was obtained by multiplying the number of RU per 2000 test cells by the number of $ESAM^{lo}$ LSK or $ESAM^{hi}$ LSK cells per BM (two femora and two tibiae) divided by 2000. For the second transplantation, two hundred $CD45.1^+$ LSK cells sorted from primary recipient mice were mixed with 1×10^5 unfractionated BM cells obtained

from WT C57BL/6-Ly5.2 (CD45.2) mice and were transplanted into irradiated C57BL/6-Ly5.2 mice. Sixteen weeks after transplantation, the contribution of CD45.1 cells to the hematopoietic reconstitution was evaluated.

Immunohistochemical analyses

Immunohistochemical staining was performed as described previously (21). In brief, bone samples were fixed in 4% paraformaldehyde and equilibrated in 30% sucrose/PBS. Fixed samples were embedded in OCT medium (Sakura Finetek, Tokyo, Japan) and frozen in cooled hexane. Sections of undecalcified femoral bone were generated via Kawamoto's film method (Cryofilm transfer kit; Leica Microsystems). The 8-μm-thick cryostat sections were first blocked with 5% FCS/PBS and then stained with mAbs. The following Abs were used for immunostaining: FITC-conjugated mAbs against Gr1, B220, CD3e, CD8, and Ter119; biotinylated mAb against Sca1; and purified mAb against ESAM. For secondary Ab, Cy3-conjugated donkey anti-rat IgG Ab was used. Biotinylated Ab was visualized with SAv-Alexa Fluor 647. The nuclei of cells were labeled with DAPI (Dojindo, Kumamoto, Japan). The sections were mounted with PermaFluor (Thermo Fisher Scientific), and confocal microscopic analyses were performed with an LSM 510 META (Carl Zeiss, Oberkochen, Germany). Image analyses were performed using an LSM image browser (Carl Zeiss).

Luciferase assays

Promoter sequences of ESAM gene were searched with Genetyx version 9 (Genetyx, Tokyo, Japan). Segments of ESAM genes were amplified by PCR and inserted in pGL3 basic vector (Promega, Madison, WI). Luciferase assays were performed using the endothelial bEnd3 cell line. The cells were seeded in 3.5-cm dishes, and 24 h later each pGL3-promoter construct and pRL-CMV encoding the *Renilla* luciferase gene were transfected into the cells by Lipofectamine. Each culture medium was changed 24 h after transfection. Luciferase assays with use of a luminometer were carried out 48 h after transfection.

Statistical analyses

Statistical analyses of chimerism status were carried out with Mann–Whitney *U* tests, and other analyses were conducted with standard Student *t* tests. Error bars used throughout indicate SD of the mean.

Results

BM injury upregulates ESAM expression on HSC

We have reported that ESAM is a durable marker for fetal and adult HSC (16). Levels decline in early postnatal life and become high again with age (16). Several Ags, including Mac1 and CD34, are known to be downregulated when fetal HSC switch to quiescent adult ones, but they emerge again on HSC as activation-related changes after myelosuppression (8, 17). We monitored ESAM expression levels in HSC-enriched fraction of adult C57BL/6 BM after a single 5-FU treatment (150 mg/kg) by flow cytometry (Fig. 1A). As shown in a previous report (8), 5-FU injection caused significant downregulation of c-Kit expression on Lin^- cells (Supplemental Fig. 1). In the same report, HSC could be enriched in the $Lin^-Sca1^+c\text{-}Kit^{dull}$ fraction after 5-FU treatment (8). Therefore, in our experiments, we applied an enlarged LSK gate covering the $c\text{-}Kit^{dull}$ HSC.

We observed remarkable increases in ESAM levels in HSC-enriched fractions from days 2–9 after a 5-FU injection (Fig. 1A). Indeed, the mean fluorescence intensity of ESAM expression on LSK increased by 11-fold in 5 d after a single 5-FU injection, compared with untreated control mice. More than 70% of LSK cells on day 5 expressed high amounts of ESAM (fluorescence intensities >10-fold the maximum level of isotype controls). After reaching peak values around days 5–6, ESAM levels gradually decreased and returned to steady-state levels by day 12.

$ESAM^{hi}$ cells formed a dominant population in the LSK fraction and logarithmically increased from day 3 to 9 in parallel with hematopoietic recovery (Fig. 1B). Quantitative real-time PCR showed gradual increases of ESAM transcripts in the LSK fraction after 5-FU treatment (Fig. 1C), suggesting that something associated with BM injury activates ESAM expression at the gene transcription level. Sublethal total body irradiation caused essentially the same change on the HSC fraction (data not shown). We evaluated ESAM levels of BM HSC fractions in BALB/c and FVB strains other than C57BL/6 mice. Expression of ESAM was also upregulated after 5-FU treatment in the $CD150^+Lin^-c\text{-}Kit^+Flt3^-$ fraction (Fig. 1D). These results suggested that BM injury upregulates ESAM levels on HSC.

Upregulation of ESAM on HSC after BM injury in comparison with other endothelial markers

Recent studies have shown that the gate of $CD150^+CD48^-$ is useful to enrich for LT-HSC activity in various contexts, from aged BM, mobilized splenocytes, or reconstituted mouse BM (1, 22). Therefore, we evaluated whether ESAM expression patterns were shared with those of SLAM family markers on adult C57BL/6 LSK cells before and after 5-FU injection. In the homeostatic BM LSK, $CD150^+CD48^-$ cells were only detectable among the $ESAM^+$ population and the percentage was higher in $ESAM^{hi}$ than $ESAM^{lo}$ (Fig. 2A, *left panels*). After 5-FU injection, more than half of LSK cells were found in the $CD150^+$ fraction, whose levels of ESAM were clearly upregulated. Additionally, percentages of the population that were $CD150^+CD48^-$ were also higher in $ESAM^{hi}$ than $ESAM^{lo}$ categories (Fig. 2A, *right panels*). With respect to mobilized LSK cells, we also detected increases of $ESAM^{hi}CD150^+$ cells in spleens and peripheral blood after day 7 from a 5-FU injection (Supplemental Fig. 2).

HSC are known to share various surface Ags with endothelial cells. We next evaluated how ESAM expression correlates with other endothelial-related HSC markers. The $ESAM^+$ LSK population in the homeostatic BM was found in $CD34^-$, $Tie2^{lo}$ $endoglin^+$, and $CD31/PECAM\text{-}1^{hi}$, which is consistent with the phenotype of adult BM LT-HSC (Fig. 2B). After 5-FU injection, the expression patterns of those markers also changed. Whereas CD34 and Tie2 showed modest increases, endoglin as well as ESAM were clearly upregulated. The CD31/PECAM-1 levels remained unchanged. These results indicate that patterns of several endothelial markers on HSC after BM injury are not homogeneous. Additionally, among the markers, ESAM appeared to be uniquely valuable for monitoring HSC activation.

$ESAM^{hi}$ HSC are actively dividing

Previous studies have proposed that BM HSC in homeostasis are quiescent, a characteristic assumed to protect them from antimetabolites such as 5-FU (4, 5, 23, 24). However, upon their activation by BM injury, it has been hypothesized that HSC move out of their homeostatic niche to proliferate and differentiate (25). To confirm that the $ESAM^{hi}$ HSC in 5-FU–treated mice are actively proliferating, we conducted cell cycle analyses. Although most $ESAM^{lo}$ and $ESAM^{hi}Sca1^+c\text{-}Kit^+$ cells after a 5-FU injection left the G_0 stage and entered into G_1 and $S+G_2+M$, the $ESAM^{hi}$ cells showed even higher percentages entering cell cycle than did the $ESAM^{lo}$ subset (Fig. 3, *upper panels*). Short-term exposure to BrdU marked more cycling cells in the $ESAM^{hi}$ fraction than in the $ESAM^{lo}$ cohort (Fig. 3, *lower panels*). $CD150^+ESAM^{hi}$ LSK cells also showed higher percentages entering cell cycle than did the $CD150^+ESAM^{lo}$ LSK cells (Supplemental Fig. 3A). Based on the fact that total stem cell activity per liver from day 12 to 16 of gestation is higher than that after day 16 (6), we compared ESAM levels in HSC fractions between embryonic day (E)14.5 and E18.5 fetal liver. ESAM levels at E14.5 were 1.9-fold higher than that at E18.5 (Supplemental Fig. 3B). These results suggest that expression of ESAM is associated with rapid division before and after birth.

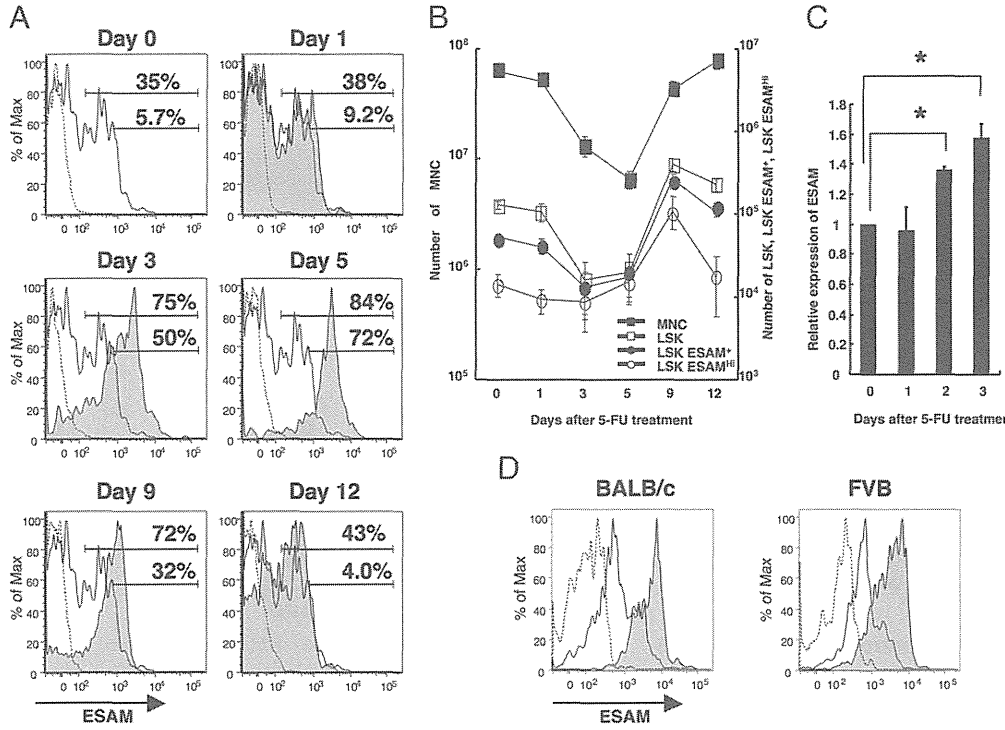

FIGURE 1. ESAM expression is upregulated on LSK cells after 5-FU treatment. (**A**) Flow cytometry analyses were performed with respect to the ESAM expression on murine BM LSK fraction through a single 5-FU (150 mg/kg) treatment. Each panel shows a representative histogram of ESAM level on LSK at days 0 (no treatment control), 1, 3, 5, 9, and 12 after a 5-FU injection. The dashed lines show background levels with an isotype control Ab. The tinted lines show ESAM levels of LSK at the indicated day after a 5-FU injection. The ESAM level of day 0 is added to each panel as an open histogram with a solid line. Upper and lower numbers in each histogram indicate the percentages of $ESAM^+$ and $ESAM^{hi}$ cells, respectively. (**B**) The numbers of total BM mononuclear cells (MNC) (■), LSK cells (□), LSK $ESAM^+$ cells (●), and LSK $ESAM^{hi}$ cells (○) from a pair of femora and tibiae were monitored after a 5-FU injection. Each point summarizes data from five mice. (**C**) Quantitative real-time PCR analyses for ESAM gene expression of LSK cells after 5-FU treatment were performed. Each bar indicates relative expression level against the expression level of day 0 (ESAM/GAPDH). (**D**) ESAM expression levels on the BM $CD150^+Lin^-c\text{-}Kit^+Flt3^-$ fraction of BALB/c and FVB mice were analyzed. The dashed lines and the solid lines show background levels and ESAM levels, respectively, on day 0. The tinted lines show ESAM levels at day 5 after a 5-FU injection (150 mg/kg). Each line of the histogram shows a representative pattern of three mice. $*p < 0.05$.

$ESAM^{hi}$ HSC have enhanced repopulating capacity

Next, we performed functional assessments of the $ESAM^{lo}$ and $ESAM^{hi}$ LSK fractions sorted from 5-FU–treated BM. In methylcellulose cultures, both fractions showed high colony-forming activities. However, whereas the $ESAM^{lo}$ fraction mainly contained committed progenitors, primitive multipotent progenitors, CFU-Mix, were significantly enriched in the $ESAM^{hi}$ fraction (Fig. 4). Additionally, those CFU-Mix cells formed high proliferative potential colonies (data not shown).

To analyze long-term reconstitution capacities in vivo, we transplanted 2000 $CD45.1^+$ $ESAM^{lo}$ or $ESAM^{hi}$ LSK cells sorted from 5-FU–treated mice, with 2×10^5 $CD45.2^+$ competitor BM cells derived from untreated mice, into lethally irradiated $CD45.2^+$ mice (Fig. 5A). Peripheral blood analyses were performed every 4 wk after transplantation, and at any time point, the mice transplanted with $ESAM^{hi}$ LSK cells showed >3-fold higher contributions of $CD45.1^+$ cells to peripheral leukocytes than did the mice transplanted with $ESAM^{lo}$ LSK cells (data not shown). Sixteen weeks after transplantation, all mice were killed and the contribution of donor type cells in BM was evaluated. The mice transplanted with $ESAM^{hi}$ cells gave significant higher levels of donor reconstitution of mononuclear, T, B, and myeloid cells (Fig. 5B). We also evaluated the contribution of $ESAM^{lo}$ and $ESAM^{hi}$ LSK populations by calculating the number of RU per BM (two femora and two tibiae). This revealed that transplanted $ESAM^{hi}$ LSK cells contained more RU per BM than did $ESAM^{lo}$ LSK cells (Fig. 5C). Additionally, recipient BM transplanted with $ESAM^{hi}$ LSK cells showed higher chimerism in the myeloid lineage, whereas $ESAM^{lo}$ LSK cells tended to reconstitute the B lineage more than did the myeloid lineage (Fig. 5D). This observation seemed to be consistent with previous reports showing that long-term reconstituting HSC predominantly contributed to the myeloid lineage (26). It is noteworthy that ESAM levels on $CD45.1^+$ donor-derived LSK cells were identical to the homeostatic level 16 wk after transplantation in the BM that was transplanted with $CD45.1^+ESAM^{hi}$ LSK cells (Fig. 5E). The $CD45.1^+$ LSK cells in the primary recipients serially reconstituted hematopoiesis in secondary $CD45.2^+$ recipients (data not shown). These results suggested that LT-HSC are enriched in the $ESAM^{hi}$ fraction of LSK cells after 5-FU injection.

Most $ESAM^{hi}$ HSC are located around perivascular areas in 5-FU–treated BM

Next, immunohistochemical analyses were conducted to locate the $ESAM^{hi}$ HSC in 5-FU–treated BM. Without treatment, $ESAM^+$ HSC were not easily distinguished because the ESAM levels were not high enough for this type of assessment (Fig. 6A, *left panels*). However, a single 5-FU treatment significantly increased ESAM expression in the HSC-enriched fraction, so that we could discriminate $ESAM^{hi}Lin^-Sca1^+$ HSC from areas with background staining (Fig. 6A). The 5-FU treatment remarkably reduced Lin^+ cells and enlarged sinusoidal vasculature spaces in BM, which favored our ability to locate the activated HSC (Fig. 6A, *right*

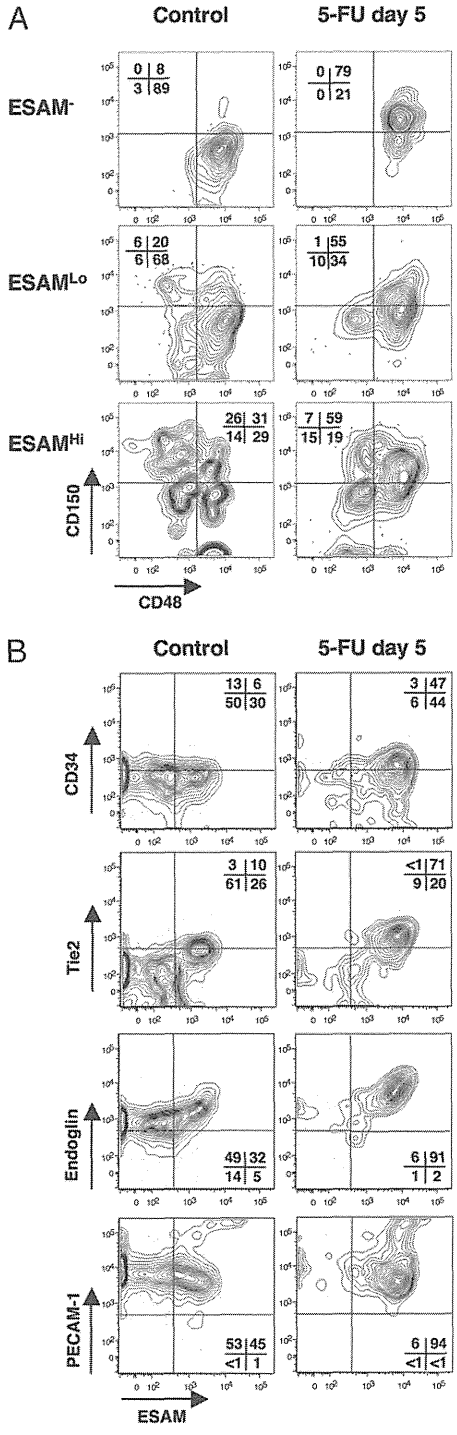

FIGURE 2. HSC express other endothelial Ags, but their patterns do not change in a homogeneous way after 5-FU treatment. (**A**) The expression levels of SLAM family markers (CD48 and CD150) on ESAM$^-$, ESAM^{lo}, and ESAM^{hi} fraction of BM LSK cells were analyzed by flow cytometry. (**B**) The expression of ESAM and endothelial-related Ags (CD34, Tie2, endoglin, and PECAM-1) on BM LSK fraction was analyzed by flow cytometry. (A and B) *Left panels* show the results of homeostatic state mice (control), and *right panels* show those of 5-FU (150 mg/kg)–treated mice (day 5). Numbers in each panel indicate the percentages of each fraction. Each panel shows a representative pattern of three mice.

panels, Supplemental Fig. 4). Note that some ESAM$^+$Sca1$^-$ cells that were not HSC were also found in these sections (Supplemental Fig. 4F). We confirmed by flow cytometry that some types of progenitors expressed low levels of ESAM after 5-FU treatment. Although megakaryocytes that were conspicuous by their morphology and very high ESAM expression distributed around the vasculature, many ESAM^{hi}Lin$^-$Sca1$^+$ cells were also found in the same area, and some of them clustered in perivascular areas (Fig. 6A, *lower right panel*). Indeed, when randomly counted, >80% of the Lin$^-$ESAM^{hi}Sca1$^+$ cells were localized within 20

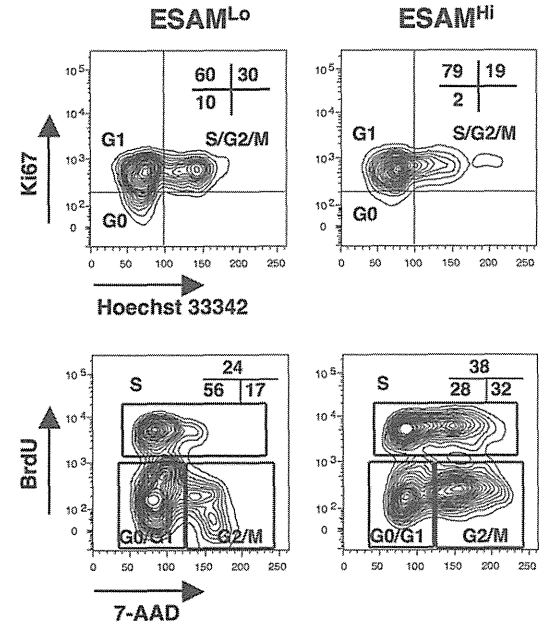

FIGURE 3. ESAM^{hi} HSC in 5-FU–treated mice are dividing. C57BL/6 mice were treated with single i.v. 150 mg/kg 5-FU, and cell cycle analyses of Sca1$^+$c-Kit$^+$ cells in BM were performed at day 5 by flow cytometry. *Upper panels* show Ki67 and Hoechst 33342 staining patterns of ESAM^{lo} or ESAM^{hi} Sca1$^+$c-Kit$^+$ fraction. Numbers in each panel indicate the percentages of G_0, G_1, or S/G_2/M fraction. *Lower panels* show the profile of BrdU and 7-aminoactinomycin D (7-AAD) stainings. BrdU was i.p. administered 12 h before analyses. Numbers in each panel indicate the percentages of G_0/G_1, S, or G_2/M fraction. The data represent three independent trials with similar results.

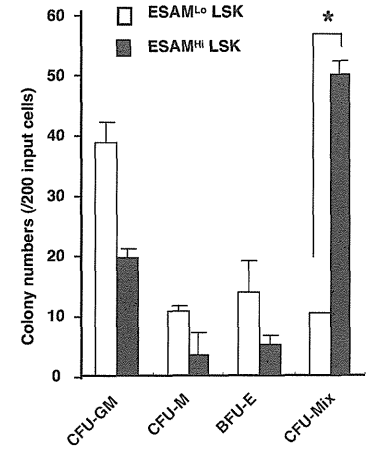

FIGURE 4. Elevated ESAM expression on LSK correlates with CFU activity. C57BL/6 mice treated with single i.v. 150 mg/kg 5-FU were killed 5 d after treatment. ESAM^{lo} or ESAM^{hi} LSK cells of BM were sorted and subjected to methylcellulose colony formation assays. Each dish contained 200 sorted cells, and colony counts were performed 9 d after culture. The bars indicate the number of CFU-GM, CFU-M, BFU-E, or CFU-Mix per one dish from ESAM^{lo} (open bar) or ESAM^{hi} (filled bar) LSK cells. The results are shown as means ± SD. The data are shown as one of two independent experiments that gave similar results. *$p < 0.05$.

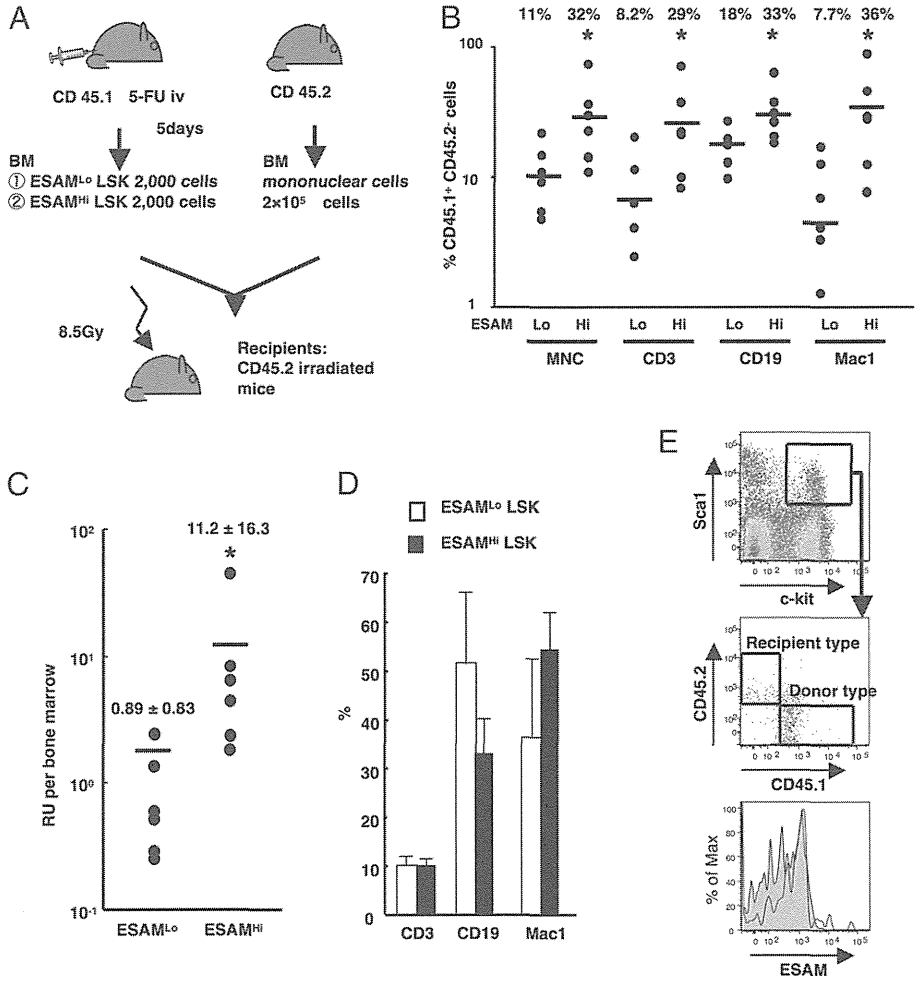

FIGURE 5. High ESAM expression correlates with long-term reconstituting HSC in 5-FU–treated mice BM. CD45.1 mice treated with single i.v. 150 mg/kg 5-FU were killed 5 d after treatment, and ESAM^{lo} or ESAM^{hi} LSK cells were sorted. Then, 2000 cells of each fraction were mixed with 2×10^5 CD45.2$^+$ whole adult BM cells and were transplanted to lethally irradiated CD45.2 WT mice (n = 6/group). (**A**) Scheme of the transplantation protocol. (**B**) Sixteen weeks after transplantation, all recipients were killed, and the contribution of transplanted CD45.1$^+$ ESAM^{lo} or ESAM^{hi} LSK cells was evaluated in BM. Percentages of the CD45.1$^+$CD45.2$^-$ population among CD45$^+$ mononuclear cells (MNC), CD3e$^+$, CD19$^+$, or Mac1$^+$ cells of each recipient were plotted. Numbers above the dots indicate mean percentages. (**C**) RU per BM of each recipient are plotted. Numbers above the dots indicate mean RU per BM ± SD. (B and C) The statistically significant differences between ESAM^{lo} and ESAM^{hi} LSK transplanted mice are shown. (**D**) The percentages of CD3e$^+$, CD19$^+$, or Mac1$^+$ cells among the CD45.1$^+$ cells of recipient BM are shown. The data from the ESAM^{lo} (open bars) and ESAM^{hi} (filled bars) LSK recipients are shown. The results are shown as means ± SD. (**E**) Flow cytometry profiles of the LSK fraction were examined in the ESAM^{hi} LSK recipients 16 wk after transplantation. The *top panel* shows the c-Kit and Sca1 expression on the Lin$^-$ fraction. The *middle panel* shows the CD45.1 and CD45.2 profile on the LSK fraction. Two frames in the *middle panel* indicate CD45.1$^+$CD45.2$^-$ LSK (donor-type) or CD45.1$^-$CD45.2$^+$ LSK (competitor-type) fraction, respectively. In the *bottom panel*, the tinted line shows the ESAM level of donor-type LSK, and the solid line shows that of competitors. The data shown represent one of two independent transplant experiments that gave similar results. *$p < 0.05$.

μm from vascular endothelium. Because the distance of 20 μm is approximate to three hematopoietic cell diameters, most activated HSC at day 5 of 5-FU treatment were probably adjacent or close to the vascular endothelium. These observations suggested that activated ESAM^{hi} HSC can be intimate with endothelial cells and/or vascular-related cells.

Hematopoietic recovery after BM stress is compromised in ESAM-deficient mice

The results above suggested that ESAM expression levels mirror HSC shifts between quiescence and activation after BM injury. However, it remained unclear whether ESAM plays any role in physiological hematopoietic recovery. To address this issue, we evaluated hematopoietic recovery of ESAM KO mice after 5-FU injection. We did not observe significant phenotypes in peripheral blood of homeostatic ESAM KO mice except for slight anemia. Intriguingly, after injecting 200 mg/kg 5-FU, the KO mice had more severe pancytopenia than did WT mice (Fig. 7A). Whereas leukocyte and platelet counts recovered by day 10, severe anemia was protracted in KO mice (hemoglobin, WT 10.4 ± 1.1 g/dl versus KO 6.0 ± 1.7 g/dl at day 10), and three of nine KO mice died before full hematopoietic recovery (Fig. 7B). With respect to the BM, ESAM deficiency did not affect numbers of total mononuclear, LSK, or Flt3$^-$ LSK cells at days 0 and 5 after 5-FU. However, all categories were significantly reduced compared with WT mice at day 8 after 5-FU (Fig. 7C). Considering that hematopoietic recovery happened after day 5, when ESAM upregulation on HSC peaked, these results suggested that ESAM is indispensable for normal hematopoietic recovery after BM injury.

NF-κB and topoisomerase II are likely important for ESAM upregulation in HSC

Next, we searched the promoter sequence of the ESAM gene to find molecular mechanisms possibly involved in ESAM upregulation

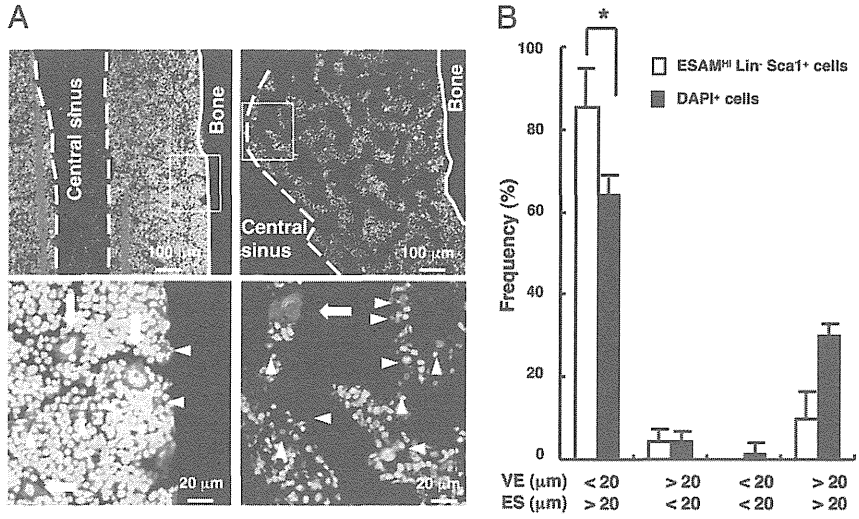

FIGURE 6. ESAM^{hi} HSC at day 5 after 5-FU injection are mainly localized around vascular areas. (**A**) BM sections from C57BL/6 mice were stained with Abs against ESAM (red), Sca1 (blue), and Lin (Gr1, B220, CD3e, CD8, and Ter119) sets (green). The nuclei of the cells are labeled with DAPI. The *left panels* are representative images of a BM section of untreated mouse, and the *right panels* are from the mouse 5 d after a 5-FU treatment (150 mg/kg). The frames in the *upper panels* are zoomed in to the *lower panels*. In the *lower panels*, ESAM^{hi} large cells are megakaryocytes (arrows). ESAM^{+}Lin^{-}Sca1^{+} cells are indicated by arrowheads. (**B**) The distances from each ESAM^{+}Lin^{-}Sca1^{+} cell to the vascular endothelium (VE) and to the endosteum (ES) were measured, and their distribution frequencies were evaluated for 5-FU–treated BM. Open bars show the frequencies for 50 ESAM^{hi}Lin^{-}Sca1^{+} cells each in four separate specimens. As controls, random 100 DAPI^{+} cells each in the same specimens were evaluated (filled bars). The cells were classified into four categories: close to VE (within 20 μm) but not close to ES (>20 μm); close to ES but not close to VE; close to both ES and VE; not close to either ES or VE. $*p < 0.05$.

(Fig. 8A). An NF-κB binding sequence at 363 bp upstream of the ESAM exon 1 drew our attention because it was well known to be an antiapoptotic factor after cell injury (27). We also found upregulation of NF-κB in the BM LSK cells after 5-FU treatment (data not shown). To examine the possible involvement of NF-κB, we administered bortezomib, a proteasome-inhibiting drug whose main action is inhibition of NF-κB, to 5-FU–treated mice (Fig. 8B). We found that bortezomib partially cancelled the ESAM upregulation caused by 5-FU injection (mean fluorescence intensity, 4790 ± 497 with 5-FU alone, 4090 ± 1050 with 5-FU and bortezomib) (Fig. 8C). Then, we conducted luciferase reporter assays to confirm the importance of the NF-κB binding sequence for ESAM transcription (Fig. 8E). We used endothelial bEnd3 cells that constantly express high levels of ESAM. The luciferase activity remarkably decreased from construct A to B (Fig. 8F).

Although the above data suggested that NF-κB was likely involved in ESAM upregulation of HSC, they also implied that other molecules should be involved. The luciferase reporter activity

A

WT	Day 0	Day 5	Day 10
WBC (/μl)	3060±684	4680±622	5160±493
RBC (×10⁴ /μl)	962±78	877±29	716±73
Hb (g/dl)	14.8±1.3	13.2±0.5	10.4±1.1
Plt (×10⁴ /μl)	87.7±8.3	52.3±6.0	171.1±36.0

ESAM KO	Day 0	Day 5	Day 10
WBC (/μl)	3540±1607	3000±212 **	4425±2642
RBC (×10⁴ /μl)	859±35 *	794±48 *	410±114 **
Hb (g/dl)	12.8±0.5 *	11.6±0.8 **	6.0±1.7 **
Plt (×10⁴ /μl)	93.1±7.9	38.3±2.0 **	213.3±38.4

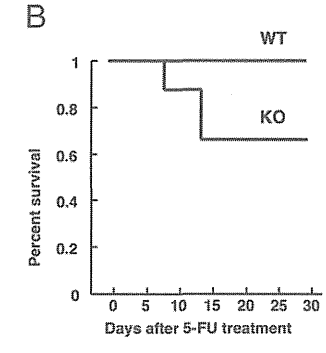

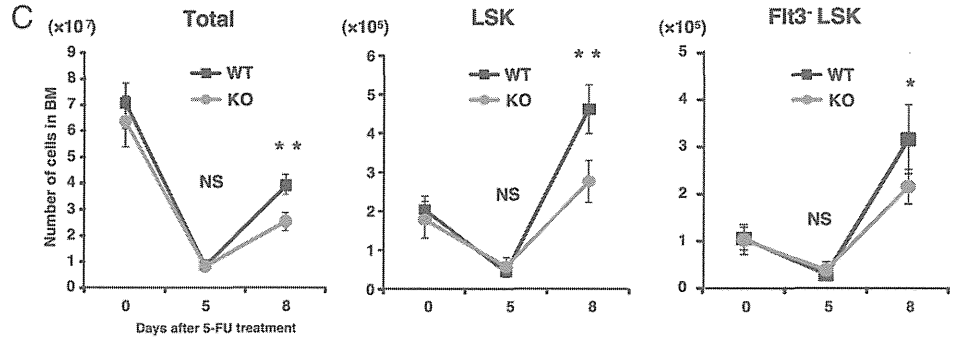

FIGURE 7. ESAM is required for normal hematopoietic recovery after BM injury. (**A**) Peripheral blood was examined every 5 d after single 200 mg/kg 5-FU treatment to WT or ESAM KO mice ($n = 5$ in each). All mice were 8-wk-old males. WBC, RBC, hemoglobin (Hb), and platelet (Plt) counts were compared between WT and ESAM KO mice at each time point. The results are shown as means ± SD. (**B**) Kaplan–Meier survival curves are shown regarding WT or ESAM KO mice treated with single 200 mg/kg 5-FU ($n = 9$ in each). (**C**) Total mononuclear cells (MNC), LSK cells, and Flt3^{-} LSK cells in BM of WT or ESAM KO mice were evaluated at day 0 (homeostatic state), day 5, and day 8 after 150 mg/kg 5-FU treatment. The results are shown as means ± SD of five mice. $*p < 0.05$, $**p < 0.01$.

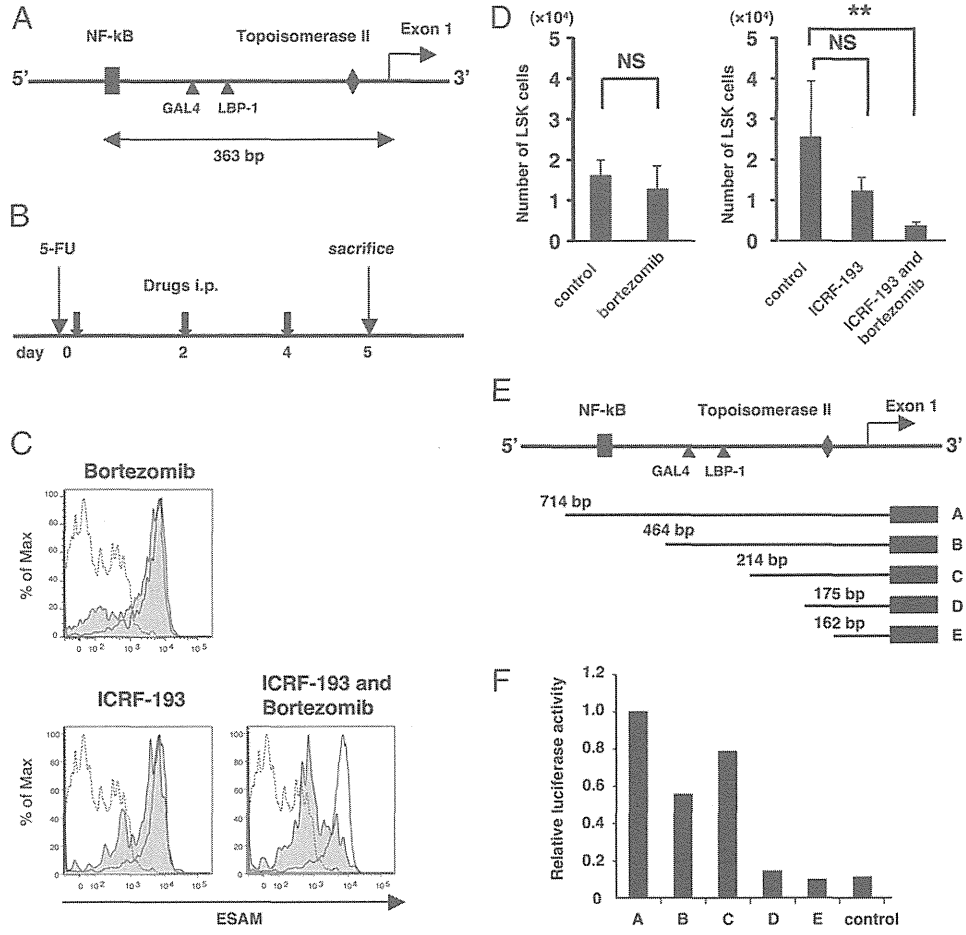

FIGURE 8. NF-κB and topoisomerase II regulate ESAM transcription. (**A**) Schematic figure regarding the upstream region of genomic ESAM DNA. Each transcription molecule is thought to work at indicated point. The distances between the beginning of topoisomerase II or NF-κB working site and the beginning of ESAM exon 1 are shown. (**B–D**) C57BL/6 mice treated with 5-FU (150 mg/kg) on day 0 were i.p. administered 1 mg/kg bortezomib and/or 6 mg/kg ICRF-193 on days 0, 2, and 4 after a 5-FU injection. Control mice were treated with solvents (saline or DMSO), in addition to 5-FU. (C) Flow cytometry analyses were performed with respect to the ESAM expression on BM LSK fraction on day 5. The dashed lines show ESAM levels of 5-FU of day 0, the open histograms with solid lines show the control ESAM levels of day 5, and the tinted lines show those of mice treated with indicated drugs after a 5-FU injection. Representative results are shown. Each group had at least three mice and showed similar results. (D) The numbers of LSK cells from a pair of femora and tibiae at day 5 of each group were evaluated. Each group had at least three mice. The results are shown as means ± SD. (**E**) Schematic figure of the luciferase assay constructs. There were topoisomerase II and NF-κB working sites upstream of exon 1 of the ESAM gene in the DNA sequence. Construct A contains both working sites. Constructs B–D contain the topoisomerase II working site. Construct E does not contain any working sites. Each DNA segment was amplified by PCR and inserted in the pGL3 basic vector. Each number (bp) is the distance from the 5′ end of each construct to the exon 1. (**F**) Luciferase assays were performed using the endothelial bEnd3 cell line. Each pGL3-promoter construct and pRL-CMV encoding the *Renilla* luciferase gene were transfected into the cells by Lipofectamine. Empty vector was used as control. Relative luciferase activity is adjusted such that construct A is 1.0. The data are shown as one of three independent experiments that gave similar results. $^{**}p < 0.01$.

sharply decreased from construct C to D probably because DNA sequences between the two are necessary for binding of the basic transcription complex. Immediately downstream of that site, we found a consensus sequence for cleavage by topoisomerase II (28). Because topoisomerase II was also known to correlate with HSC activation, we tested ICRF-193, a topoisomerase II-specific inhibitor, in 5-FU–treated mice. Similar to bortezomib, ICRF-193 partially inhibited the ESAM upregulation (mean fluorescence intensity, 3260 ± 685 with 5-FU and ICRF-193) (Fig. 8C). Interestingly, the ESAM upregulation was remarkably abrogated when bortezomib and ICRF-193 were administered simultaneously (mean fluorescence intensity, 1980 ± 392 with 5-FU, bortezomib, and ICRF-193) (Fig. 8C). The mice treated with bortezomib and ICRF-193 showed significant reduction of LSK cells compared with control mice at day 5, although the mice treated with a single inhibitory drug did not respond in that way (Fig. 8D). These results indicated that NF-κB and topoisomerase II synergistically regulate ESAM expression on HSC after BM injury.

Discussion

Although adult stem cells divide infrequently, they have high proliferative capacity. Emerging evidence suggests that both quiescent and active stem cells simultaneously exist in different but consecutive niches under normal steady-state conditions (9). It is also well known that the quiescent stem cells proliferate after wounding or transplantation (5, 29). Accurate identification of stem cells according to their proliferative states is essential to understand the biological nature of "stemness" and to develop tissue-regeneration therapies. We now report that ESAM, a new marker for HSC, represents a powerful tool to monitor the transition of HSC between quiescence and activation after BM injury. Furthermore, ESAM is required for normal recovery from marrow ablation.

Treatment of mice with 5-FU enriches primitive HSC by eliminating most proliferating progenitors while sparing non-cycling quiescent HSC. Additionally, 5-FU has been widely used to stimulate quiescent adult HSC to proliferate (8, 30–33). In the present study, we exploited this method to evaluate whether ESAM levels would change, and we observed dramatic upregulation. Previous studies showed that expression levels of many adult HSC markers change during hematopoietic recovery after 5-FU–mediated myeloablation. Whereas expression of c-Kit and N-cadherin decrease, levels of Mac1, CD34, and AA4 that are markers for fetal HSC revive (8, 31, 33). CD150 and Sca1 are also known to increase on activated HSC, as confirmed in our study (see Fig. 2A, Supplemental Fig. 1). However, we stress that the degree of change in ESAM greatly exceeds that of other markers. The ESAM^{hi} LSK fraction includes more LT-HSC defined by SLAM markers than does the ESAM^{lo} subset (Fig. 2A, *right panels*). However, it is controversial whether HSC can only be found in the CD150^{+} fraction (34, 35). For that reason, we did not use SLAM family markers to purify HSC when analyzing functions of ESAM.

Our cell cycle analyses showed that virtually all ESAM^{hi}Sca1^{+}c-Kit^{+} cells after 5-FU treatment exit the G_0 phase (Fig. 3). Alternatively, long-term repopulating HSC can be enriched in the ESAM^{hi} fraction (Fig. 5B, 5C). These results suggest that the ESAM^{hi} LSK fraction includes cycling, long-term multipotent HSC. Our data are in accordance with a previous report by Haug et al. (31) showing that the N-cadherin^{lo} HSC in 5-FU–treated BM have high cell cycle entry rates and, at the same time, robust long-term reconstituting potential. These features do not match those of adult HSC under steady-state, but rather are reminiscent of fetal HSC. It is interesting that activated adult HSC after BM injury resemble fetal HSC regarding not only cell cycle status but also surface markers.

Although it was reported that the LSK Thy1^{lo} Flk2/Flt3^{-} fraction in mobilized BM contains authentic HSC less frequently than those in untreated BM (36), our present data have demonstrated that HSC of 5-FU–treated BM can effectively reconstitute long-term hematopoiesis. One interpretation for the discrepancy is that because the HSC change their phenotype by activation, our sorting method, which depended on high expression of ESAM, might have enriched the authentic HSC more efficiently than did the conventional sorting gate. Another possibility is that active cycling and good engraftment may not be mutually exclusive. Indeed, some previous reports showed that cycling HSC are not necessarily incapable of engraftment when transplanted (37, 38). Transplanted ESAM^{hi} LSK cells reconstituted the ESAM^{lo} LSK fraction in lethally irradiated recipients 16 wk after transplantation, suggesting that the ESAM^{hi} subset could keep its stemness even after entering cell cycle. Of note, ESAM levels return to homeostatic levels by 12 d after 5-FU injection.

Previous studies used high-resolution real-time imaging systems to show that transplanted HSC tend to first home to the endosteum in irradiated mice (39, 40). Our immunohistochemical analyses showed that most ESAM^{hi} HSC in BM at day 5 following 5-FU treatment were localized within 20 μm from vascular endothelium. As previously predicted by Venezia et al. (33), quiescent HSC might need to once pause in the endosteum so that they can prepare to proliferate. After receiving unknown signals, they migrate to a proliferative zone, which is presumably composed of vascular endothelial cells. ESAM might help HSC to receive the proliferative signals from ESAM^{+} endothelial cells because ESAM mediates cell–cell adhesion through homophilic interactions (11). Alternatively, the endosteum and the sinusoidal vascular area might cooperatively form a proliferative environment for HSC. We observed that sinusoidal vasculature spaces and perivascular areas are remarkably enlarged in BM after 5-FU treatment (Fig. 6A). Indeed, a previous study showed that many osteoblasts are adjacent to or in proximity to vasculature in 5-FU–treated BM (39). Therefore, the ESAM^{hi} HSC interacting with endothelial cells simultaneously may receive signals from endosteal niches. Recently, it has been reported that the nervous system and glial cells play important roles in the HSC niche (41, 42). It would be important to examine how the ESAM^{hi} HSC interact with CXCL12-abundant reticular cells or glial cells because they are key components of both HSC niches (21).

Additional endothelial or other Ags whose expression levels are enhanced by BM injury might be functionally involved in activated HSC. However, no apparent phenotypes with either CD34 or CD150 KO mice have been documented (1, 43). In contrast, our new findings strongly suggest that ESAM is indispensable for normal hematopoietic recovery after BM injury. ESAM KO mice do not show hematopoietic defects except for slight anemia (Fig. 7) (44). However, hematopoietic recovery after BM injury was significantly compromised in the ESAM KO mice, suggesting its importance under stress conditions. Especially, the deficiency caused significant anemia after 5-FU treatment, and some KO mice with severe anemia died before BM recovery. Thus, ESAM might be particularly important for demand erythropoiesis. Because ESAM^{hi} HSC closely interact with ESAM^{+} vascular endothelial cells (Fig. 6), HSC might receive necessary signals directly or indirectly via interaction with ESAM. In fact, ESAM deficiency resulted in insufficient Rho signaling in endothelial cells, which potentially regulates the stabilization of endothelial tight junctions (13). Rho is also expressed in hematopoietic progenitors and involved in their polarity and mobility (45). Further studies are necessary to learn precisely how ESAM controls HSC function during BM recovery.

It is very important to know how ESAM expression is regulated in HSC. NF-κB is known to be activated by BM stress and induces cyclin D1, a key regulator of the G_1 check point (46). Indeed, we observed upregulation of NF-κB in HSC after 5-FU treatment (data not shown). Topoisomerase II is required for the G_0-to-S phase transition in mammalian cells (47). NF-κB was implicated as a key ESAM transcription factor by luciferase assay (Fig. 8F). In addition to NF-κB, we focused on topoisomerase II, because this enzyme is required for regulated transcription (48). Although independent administration of inhibitors for each factor showed only subtle effects on ESAM levels, the drugs synergistically but still partially abrogated the ESAM upregulation in 5-FU–treated HSC (Fig. 8C). Decreased ESAM expression with combined bortezomib and ICRF-193 treatment had a suppressive effect on the number of LSK cells, although treatment of a single inhibitory drug did not have significant effects (Fig. 8D). Given that ESAM KO mice did not show significant cytopenia at 5-FU day 5 compared with WT mice (Fig. 7C), bortezomib and ICRF-193 may suppress cell cycle-related pathways other than ESAM. Recently, reactive oxygen species (ROS) are attracting attention because levels in HSC influence their cell cycle status, self-renewal ability, and differentiation potential (49, 50). Accumulation of ROS is known to activate NF-κB signaling (51). Additionally, several studies have suggested that accumulation of ROS is likely involved in HSC aging (52–54). We reported that whereas ESAM levels on the LSK fraction decrease after the neonatal period, they increase again with aging (16). Bowie et al. (7) previously proved that fetal type HSC change their self-renewal and differentiation properties to be quiescent at 4 wk after birth when blood cell outputs reach homeostasis. Alternatively, several reports showed that absolute numbers of phenotypic HSC increase by 3- to 10-

fold in aged mouse BM (55–57). At present, we are studying whether intracellular ROS levels and related signaling pathways might be involved in ESAM fluctuation on HSC, not only after BM stress but also in the context of aging.

In summary, our data have shown that ESAM can be valuable for purifying proliferating HSC. Information from those HSC will give us important insights regarding essential molecules for HSC expansion. Additionally, the data from ESAM KO mice have suggested that high ESAM expression on HSC is likely to play important roles for hematopoietic recovery after BM injury. Further studies should address physiological meanings of the fluctuation of ESAM levels according to the HSC status.

Acknowledgments

We thank Drs. Stefan Butz and Dietmar Vestweber (Max Planck Institute) for a rat anti-mouse ESAM Ab and Drs. Michiko Ichii and Paul W. Kincade for many thoughtful suggestions on the manuscript.

Disclosures

The authors have no financial conflicts of interest.

References

1. Kiel, M. J., O. H. Yilmaz, T. Iwashita, O. H. Yilmaz, C. Terhorst, and S. J. Morrison. 2005. SLAM family receptors distinguish hematopoietic stem and progenitor cells and reveal endothelial niches for stem cells. *Cell* 121: 1109–1121.
2. Osawa, M., K. Hanada, H. Hamada, and H. Nakauchi. 1996. Long-term lymphohematopoietic reconstitution by a single CD34-low/negative hematopoietic stem cell. *Science* 273: 242–245.
3. Spangrude, G. J., S. Heimfeld, and I. L. Weissman. 1988. Purification and characterization of mouse hematopoietic stem cells. *Science* 241: 58–62.
4. Foudi, A., K. Hochedlinger, D. Van Buren, J. W. Schindler, R. Jaenisch, V. Carey, and H. Hock. 2009. Analysis of histone 2B-GFP retention reveals slowly cycling hematopoietic stem cells. *Nat. Biotechnol.* 27: 84–90.
5. Wilson, A., E. Laurenti, G. Oser, R. C. van der Wath, W. Blanco-Bose, M. Jaworski, S. Offner, C. F. Dunant, L. Eshkind, E. Bockamp, et al. 2008. Hematopoietic stem cells reversibly switch from dormancy to self-renewal during homeostasis and repair. *Cell* 135: 1118–1129.
6. Ema, H., and H. Nakauchi. 2000. Expansion of hematopoietic stem cells in the developing liver of a mouse embryo. *Blood* 95: 2284–2288.
7. Bowie, M. B., D. G. Kent, B. Dykstra, K. D. McKnight, L. McCaffrey, P. A. Hoodless, and C. J. Eaves. 2007. Identification of a new intrinsically timed developmental checkpoint that reprograms key hematopoietic stem cell properties. *Proc. Natl. Acad. Sci. USA* 104: 5878–5882.
8. Randall, T. D., and I. L. Weissman. 1997. Phenotypic and functional changes induced at the clonal level in hematopoietic stem cells after 5-fluorouracil treatment. *Blood* 89: 3596–3606.
9. Li, L., and H. Clevers. 2010. Coexistence of quiescent and active adult stem cells in mammals. *Science* 327: 542–545.
10. Wilson, A., and A. Trumpp. 2006. Bone-marrow haematopoietic-stem-cell niches. *Nat. Rev. Immunol.* 6: 93–106.
11. Hirata Ki, T., K. Ishida, M. Penta, E. Rezaee, J. Yang, Wohlgemuth, and T. Quertermous. 2001. Cloning of an immunoglobulin family adhesion molecule selectively expressed by endothelial cells. *J. Biol. Chem.* 276: 16223–16231.
12. Nasdala, I., K. Wolburg-Buchholz, H. Wolburg, A. Kuhn, K. Ebnet, G. Brachtendorf, U. Samulowitz, B. Kuster, B. Engelhardt, D. Vestweber, and S. Butz. 2002. A transmembrane tight junction protein selectively expressed on endothelial cells and platelets. *J. Biol. Chem.* 277: 16294–16303.
13. Wegmann, F., B. Petri, A. G. Khandoga, C. Moser, A. Khandoga, S. Volkery, H. Li, I. Nasdala, O. Brandau, R. Fässler, et al. 2006. ESAM supports neutrophil extravasation, activation of Rho, and VEGF-induced vascular permeability. *J. Exp. Med.* 203: 1671–1677.
14. Hara, T., T. Ishida, H. M. Cangara, and K. Hirata. 2009. Endothelial cell-selective adhesion molecule regulates albuminuria in diabetic nephropathy. *Microvasc. Res.* 77: 348–355.
15. Stalker, T. J., J. Wu, A. Morgans, E. A. Traxler, L. Wang, M. S. Chatterjee, D. Lee, T. Quertermous, R. A. Hall, D. A. Hammer, et al. 2009. Endothelial cell specific adhesion molecule (ESAM) localizes to platelet-platelet contacts and regulates thrombus formation in vivo. *J. Thromb. Haemost.* 7: 1886–1896.
16. Yokota, T., K. Oritani, S. Butz, K. Kokame, P. W. Kincade, T. Miyata, D. Vestweber, and Y. Kanakura. 2009. The endothelial antigen ESAM marks primitive hematopoietic progenitors throughout life in mice. *Blood* 113: 2914–2923.
17. Ogawa, M. 2002. Changing phenotypes of hematopoietic stem cells. *Exp. Hematol.* 30: 3–6.
18. Ishida, T., R. K. Kundu, E. Yang, K. Hirata, Y. D. Ho, and T. Quertermous. 2003. Targeted disruption of endothelial cell-selective adhesion molecule inhibits angiogenic processes in vitro and in vivo. *J. Biol. Chem.* 278: 34598–34604.
19. Inoue, M., T. Ishida, T. Yasuda, R. Toh, T. Hara, H. M. Cangara, Y. Rikitake, K. Taira, L. Sun, R. K. Kundu, et al. 2010. Endothelial cell-selective adhesion molecule modulates atherosclerosis through plaque angiogenesis and monocyte-endothelial interaction. *Microvasc. Res.* 80: 179–187.
20. Harrison, D. E., C. T. Jordan, R. K. Zhong, and C. M. Astle. 1993. Primitive hemopoietic stem cells: direct assay of most productive populations by competitive repopulation with simple binomial, correlation and covariance calculations. *Exp. Hematol.* 21: 206–219.
21. Sugiyama, T., H. Kohara, M. Noda, and T. Nagasawa. 2006. Maintenance of the hematopoietic stem cell pool by CXCL12-CXCR4 chemokine signaling in bone marrow stromal cell niches. *Immunity* 25: 977–988.
22. Yilmaz, O. H., M. J. Kiel, and S. J. Morrison. 2006. SLAM family markers are conserved among hematopoietic stem cells from old and reconstituted mice and markedly increase their purity. *Blood* 107: 924–930.
23. Arai, F., and T. Suda. 2007. Maintenance of quiescent hematopoietic stem cells in the osteoblastic niche. *Ann. N. Y. Acad. Sci.* 1106: 41–53.
24. Lerner, C., and D. E. Harrison. 1990. 5-Fluorouracil spares hemopoietic stem cells responsible for long-term repopulation. *Exp. Hematol.* 18: 114–118.
25. Yin, T., and L. Li. 2006. The stem cell niches in bone. *J. Clin. Invest.* 116: 1195–1201.
26. Morita, Y., H. Ema, and H. Nakauchi. 2010. Heterogeneity and hierarchy within the most primitive hematopoietic stem cell compartment. *J. Exp. Med.* 207: 1173–1182.
27. Wang, C. Y., J. C. Cusack, Jr., R. Liu, and A. S. Baldwin, Jr. 1999. Control of inducible chemoresistance: enhanced anti-tumor therapy through increased apoptosis by inhibition of NF-κB. *Nat. Med.* 5: 412–417.
28. Spitzner, J. R., and M. T. Muller. 1988. A consensus sequence for cleavage by vertebrate DNA topoisomerase II. *Nucleic Acids Res.* 16: 5533–5556.
29. Tumbar, T., G. Guasch, V. Greco, C. Blanpain, W. E. Lowry, M. Rendl, and E. Fuchs. 2004. Defining the epithelial stem cell niche in skin. *Science* 303: 359–363.
30. Harrison, D. E., and C. P. Lerner. 1991. Most primitive hematopoietic stem cells are stimulated to cycle rapidly after treatment with 5-fluorouracil. *Blood* 78: 1237–1240.
31. Haug, J. S., X. C. He, J. C. Grindley, J. P. Wunderlich, K. Gaudenz, J. T. Ross, A. Paulson, K. P. Wagner, Y. Xie, R. Zhu, et al. 2008. N-cadherin expression level distinguishes reserved versus primed states of hematopoietic stem cells. *Cell Stem Cell* 2: 367–379.
32. Sirin, O., G. L. Lukov, R. Mao, O. M. Conneely, and M. A. Goodell. 2010. The orphan nuclear receptor Nurr1 restricts the proliferation of haematopoietic stem cells. *Nat. Cell Biol.* 12: 1213–1219.
33. Venezia, T. A., A. A. Merchant, C. A. Ramos, N. L. Whitehouse, A. S. Young, C. A. Shaw, and M. A. Goodell. 2004. Molecular signatures of proliferation and quiescence in hematopoietic stem cells. *PLoS Biol.* 2: e301.
34. Kiel, M. J., O. H. Yilmaz, and S. J. Morrison. 2008. $CD150^-$ cells are transiently reconstituting multipotent progenitors with little or no stem cell activity. *Blood* 111: 4413–4414, author reply 4414–4415.
35. Weksberg, D. C., S. M. Chambers, N. C. Boles, and M. A. Goodell. 2008. $CD150^-$ side population cells represent a functionally distinct population of long-term hematopoietic stem cells. *Blood* 111: 2444–2451.
36. Passegué, E., A. J. Wagers, S. Giuriato, W. C. Anderson, and I. L. Weissman. 2005. Global analysis of proliferation and cell cycle gene expression in the regulation of hematopoietic stem and progenitor cell fates. *J. Exp. Med.* 202: 1599–1611.
37. Steinman, R. A. 2002. Cell cycle regulators and hematopoiesis. *Oncogene* 21: 3403–3413.
38. Wilpshaar, J., J. H. Falkenburg, X. Tong, W. A. Noort, R. Breese, D. Heilman, H. Kanhai, C. M. Orschell-Traycoff, and E. F. Srour. 2000. Similar repopulating capacity of mitotically active and resting umbilical cord blood $CD34^+$ cells in NOD/SCID mice. *Blood* 96: 2100–2107.
39. Lo Celso, C., H. E. Fleming, J. W. Wu, C. X. Zhao, S. Miake-Lye, J. Fujisaki, D. Côté, D. W. Rowe, C. P. Lin, and D. T. Scadden. 2009. Live-animal tracking of individual haematopoietic stem/progenitor cells in their niche. *Nature* 457: 92–96.
40. Xie, Y., T. Yin, W. Wiegraebe, X. C. He, D. Miller, D. Stark, K. Perko, R. Alexander, J. Schwartz, J. C. Grindley, et al. 2009. Detection of functional haematopoietic stem cell niche using real-time imaging. *Nature* 457: 97–101.
41. Katayama, Y., M. Battista, W. M. Kao, A. Hidalgo, A. J. Peired, S. A. Thomas, and P. S. Frenette. 2006. Signals from the sympathetic nervous system regulate hematopoietic stem cell egress from bone marrow. *Cell* 124: 407–421.
42. Yamazaki, S., H. Ema, G. Karlsson, T. Yamaguchi, H. Miyoshi, S. Shioda, M. M. Taketo, S. Karlsson, A. Iwama, and H. Nakauchi. 2011. Nonmyelinating Schwann cells maintain hematopoietic stem cell hibernation in the bone marrow niche. *Cell* 147: 1146–1158.
43. Cheng, J., S. Baumhueter, G. Cacalano, K. Carver-Moore, H. Thibodeaux, R. Thomas, H. E. Broxmeyer, S. Cooper, N. Hague, M. Moore, and L. A. Lasky. 1996. Hematopoietic defects in mice lacking the sialomucin CD34. *Blood* 87: 479–490.
44. Ooi, A. G., H. Karsunky, R. Majeti, S. Butz, D. Vestweber, T. Ishida, T. Quertermous, I. L. Weissman, and E. C. Forsberg. 2009. The adhesion molecule Esam1 is a novel hematopoietic stem cell marker. *Stem Cells* 27: 653–661.
45. Fonseca, A. V., D. Freund, M. Bornhäuser, and D. Corbeil. 2010. Polarization and migration of hematopoietic stem and progenitor cells rely on the RhoA/ROCK I pathway and an active reorganization of the microtubule network. *J. Biol. Chem.* 285: 31661–31671.
46. Hinz, M., D. Krappmann, A. Eichten, A. Heder, C. Scheidereit, and M. Strauss. 1999. NF-κB function in growth control: regulation of cyclin D1 expression and G_0/G_1-to-S-phase transition. *Mol. Cell. Biol.* 19: 2690–2698.

47. Hossain, M. S., N. Akimitsu, T. Takaki, H. Hirai, and K. Sekimizu. 2002. ICRF-193, a catalytic inhibitor of DNA topoisomerase II, inhibits re-entry into the cell division cycle from quiescent state in mammalian cells. *Genes Cells* 7: 285–294.
48. Ju, B. G., V. V. Lunyak, V. Perissi, I. Garcia-Bassets, D. W. Rose, C. K. Glass, and M. G. Rosenfeld. 2006. A topoisomerase IIβ-mediated dsDNA break required for regulated transcription. *Science* 312: 1798–1802.
49. Jang, Y. Y., and S. J. Sharkis. 2007. A low level of reactive oxygen species selects for primitive hematopoietic stem cells that may reside in the low-oxygenic niche. *Blood* 110: 3056–3063.
50. Orford, K. W., and D. T. Scadden. 2008. Deconstructing stem cell self-renewal: genetic insights into cell-cycle regulation. *Nat. Rev. Genet.* 9: 115–128.
51. Morgan, M. J., and Z. G. Liu. 2011. Crosstalk of reactive oxygen species and NF-κB signaling. *Cell Res.* 21: 103–115.
52. Ito, K., A. Hirao, F. Arai, S. Matsuoka, K. Takubo, I. Hamaguchi, K. Nomiyama, K. Hosokawa, K. Sakurada, N. Nakagata, et al. 2004. Regulation of oxidative stress by ATM is required for self-renewal of haematopoietic stem cells. *Nature* 431: 997–1002.
53. Liu, J., L. Cao, J. Chen, S. Song, I. H. Lee, C. Quijano, H. Liu, K. Keyvanfar, H. Chen, L. Y. Cao, et al. 2009. Bmi1 regulates mitochondrial function and the DNA damage response pathway. *Nature* 459: 387–392.
54. Tothova, Z., R. Kollipara, B. J. Huntly, B. H. Lee, D. H. Castrillon, D. E. Cullen, E. P. McDowell, S. Lazo-Kallanian, I. R. Williams, C. Sears, et al. 2007. FoxOs are critical mediators of hematopoietic stem cell resistance to physiologic oxidative stress. *Cell* 128: 325–339.
55. Kim, M., H. B. Moon, and G. J. Spangrude. 2003. Major age-related changes of mouse hematopoietic stem/progenitor cells. *Ann. N. Y. Acad. Sci.* 996: 195–208.
56. Morrison, S. J., A. M. Wandycz, K. Akashi, A. Globerson, and I. L. Weissman. 1996. The aging of hematopoietic stem cells. *Nat. Med.* 2: 1011–1016.
57. Sudo, K., H. Ema, Y. Morita, and H. Nakauchi. 2000. Age-associated characteristics of murine hematopoietic stem cells. *J. Exp. Med.* 192: 1273–1280.

PLATELETS AND THROMBOPOIESIS

Recognition of highly restricted regions in the β-propeller domain of αIIb by platelet-associated anti-αIIbβ3 autoantibodies in primary immune thrombocytopenia

Kazunobu Kiyomizu,[1] Hirokazu Kashiwagi,[1] Tsuyoshi Nakazawa,[1] Seiji Tadokoro,[1] Shigenori Honda,[2] Yuzuru Kanakura,[1] and Yoshiaki Tomiyama[1,3]

[1]Department of Hematology and Oncology, Osaka University Graduate School of Medicine, Osaka, Japan; [2]Department of Molecular Pathogenesis, National Cerebral and Cardiovascular Center, Osaka, Japan; and [3]Department of Blood Transfusion, Osaka University Hospital, Osaka, Japan

Platelet-associated (PA) IgG autoantibodies play an essential role in primary immune thrombocytopenia (ITP). However, little is known about the epitopes of these Abs. This study aimed to identify critical binding regions for PA anti-αIIbβ3 Abs. Because PA anti-αIIbβ3 Abs bound poorly to mouse αIIbβ3, we created human-mouse chimera constructs. We first examined 76 platelet eluates obtained from patients with primary ITP. Of these, 26 harbored PA anti-αIIbβ3 Abs (34%). Further analysis of 15 patients who provided sufficient materials showed that the epitopes of these Abs were mainly localized in the N-terminal half of the β-propeller domain in αIIb (L1-W235). We could identify 3 main recognition sites in the region; 2 eluates recognized a conformation formed by the W1:1-2 and W2:3-4 loops, 5 recognized W1:2-3, and 4 recognized W3:4-1. The remaining 4 eluates could not be defined by the binding sites. Within these regions, we identified residues critical for binding, including S29 and R32 in W1:1-2; G44 and P45 in W1:2-3; and P135, E136, and R139 in W2:3-4. Of 11 eluates whose recognition sites were identified, 5 clearly showed restricted κ/λ-chain usage. These results suggested that PA anti-αIIbβ3 Abs in primary ITP tended to recognize highly restricted regions of αIIb with clonality. (*Blood*. 2012;120(7):1499-1509)

Introduction

Primary immune thrombocytopenia (ITP) is an autoimmune disorder characterized by thrombocytopenia that results from immune-mediated platelet destruction and reduced platelet production.[1-4] In ITP, autoantibodies bound to platelets (platelet-associated antibodies; PA Abs) cause platelet destruction by Fcγ receptor–mediated phagocytosis.[1] Furthermore, autoantibodies binding to megakaryocytes led to decreased maturation and cell death.[5,6] Multiple targets of autoantibodies have been found in ITP. Among patients with chronic ITP, 43%-57% and 18%-50% harbored PA Abs that recognized the platelet membrane glycoprotein (GP) IIb/IIIa (integrin αIIbβ3) and the GPIb/IX/V complex, respectively.[7-10]

For more than 2 decades, efforts have been focused on identifying the target epitopes for PA Abs to improve our understanding of the pathogenesis of primary ITP and to pursue a therapeutic approach. We and others previously reported that, in chronic ITP, PA anti-αIIbβ3 Abs frequently bound to cation-dependent conformational antigens and did not react with αvβ3.[11-13] Those data suggested that, in primary ITP, the target epitopes of anti-αIIbβ3 Abs may be localized mainly on αIIb; in contrast, in HIV-associated ITP, the target epitopes appeared to be localized to the 49-66 residues of β3.[14] Moreover, we previously reported that, in one-third of patients with ITP (11 of 34), PA anti-αIIbβ3 Ab binding was markedly impaired against KO variant αIIbβ3, which had 2 amino acids inserted between residues 160 and 161 in the W3:4-1 loop of the β-propeller domain.[15] However, target epitopes of most PA anti-αIIbβ3 Abs remain to be elucidated.

PA anti-αIIbβ3 Abs typically recognize conformational epitopes, rather than linear epitopes.[16,17] Therefore, epitope mapping for PA Abs requires the retention of major conformations in αIIbβ3. Because we noticed that the PA anti-αIIbβ3 Abs from patients with ITP had markedly impaired reactivity to mouse αIIbβ3, we characterized target epitopes of PA anti-αIIbβ3 Abs by exploring their reactivity to the cells that expressed human-mouse chimeric αIIbβ3 in the present study. A thorough analysis of 15 eluates obtained from patients with primary ITP found that most of the PA anti-αIIbβ3 Abs recognized the N-terminal half of the β-propeller domain in αIIb. We identified 3 main Ab recognition sites in the region and residues that were critical for the binding of some Abs.

Methods

Patients

We first examined 76 eluates obtained from patients with primary ITP (21 men, 55 women). Diagnosis of primary ITP was based on a report from an international working group.[18] We obtained written, informed consent for blood sampling necessary for this study from all patients, in accordance with the Declaration of Helsinki. This study was approved by the Osaka University Institutional Review Board. With the use of flow cytometry with 293T cells expressing αIIbβ3, we detected anti-αIIbβ3 autoantibodies in 26 of 76 (34%) platelet eluates (6 and 20 eluates were obtained from men and women, respectively). Of these 26 eluates, we further analyzed 15 patients who provided sufficient quantity of platelet eluates for this study. The characteristics of these 15 patients (PTs) are shown in Table 1. Although 5 eluates were

Submitted February 8, 2012; accepted June 12, 2012. Prepublished online as *Blood* First Edition paper, June 22, 2012; DOI 10.1182/blood-2012-02-409995.

The online version of this article contains a data supplement.

The publication costs of this article were defrayed in part by page charge payment. Therefore, and solely to indicate this fact, this article is hereby marked "advertisement" in accordance with 18 USC section 1734.

Table 1. Clinical profiles of 15 patients with ITP at blood sampling

PT no.	Age, y	Sex	Plt count, $\times 10^3/\mu L$	Medications	Splenectomy	Duration of ITP
1	71	F	189-311	P	No	1 mo
2	63	F	14-212	SB+P	Yes	> 10 y
3	37	F	5-199	SB+P	Yes	> 10 y
5	65	F	64-116	P	No	6-10 y
6	49	F	189	P	No	1 mo
7*	55	M	103-105	N	Yes	> 10 y
12*	56	F	22-116	SB+P	Yes	> 10 y
17	64	F	23-146	SB+P	Yes	> 10 y
23	75	F	41-97	N	No	1-5 y
34	67	M	17-144	P	No	4-8 mo
36	72	F	76-186	P+IV	No	1-3 mo
37	62	F	27	P	Yes	> 10 y
41	53	F	40-55	SB+P	Yes	> 10 y
42	42	F	128-271	SB	Yes	> 10 y
45	73	F	17-203	P+IV	No	3-7 mo

Plt indicates platelet; P, prednisolone; SB, eltrombopag; N, none, and IV, intravenous gamma globulin.

*PTs 7 and 12 were studied in our previous reports as nos. 2 and 6, respectively.[15]

obtained < 12 months after the ITP diagnosis, all (except PT 36) were classified as chronic ITP.[18] PT 7 and PT 12 were studied in our previous report.[15] The binding of PA anti-αIIbβ3 Ab of PT 12 was markedly impaired by the KO mutation in αIIb, whereas that of PT 7 was not affected by the mutation.

Platelet isolation and preparation of PA antibodies

Platelets and platelet eluates were prepared as previously described.[19] In brief, washed platelets were obtained by differential centrifugation and adjusted to a concentration of $200 \times 10^3/\mu L$ in PBS. PA Abs were eluted by vigorous mixing with an equal amount of diethyl ether. Platelet eluates were maintained at −80°C until use.

Construction of expression vectors

The N-terminal portion of αIIb, known as the β-propeller domain, contains 7 radially arranged β-sheets, termed "W" because of their topology. Each W structure has 4 anti-parallel β-strands and 4 connecting loops.[20] Figure 1A shows the human and mouse sequence alignment of the β-propeller domains. The boxes indicate the small loop structures of each β-sheet domain, and the asterisks indicate amino acid differences between the human and mouse sequences. Human *αIIb* and *β3* cDNAs cloned into the pcDNA3 vector were gifts from Dr Peter Newman and Dr Gilbert White (BloodCenter of Wisconsin), respectively. Mouse *αIIb* and *β3* cDNAs were obtained by reverse transcribing platelet RNA from C57BL/6 mice, amplifying by PCR, and subcloning into the pcDNA3 expression vector. αIIb expression vectors with swapped human and mouse cassettes were constructed with the megaprimer PCR method[21] or with a site-directed mutagenesis kit (Agilent Technologies). The entire mutated αIIb sequence was confirmed for each vector. The swapping mutants are shown in Figure 1B. The m(X)H expressed the human αIIb that carried the mouse sequences from the N-terminus to the X region; conversely, H(X)m expressed mouse αIIb that carried the human sequences from the N-terminus to the X region. Hm(X)H expressed human αIIb in which the only X region was swapped with the corresponding region from mouse αIIb. mH(X-Y)m expressed mouse αIIb with a large part of the N-terminal region (X to Y) swapped with the corresponding region from human αIIb. m(β-propeller)H expressed the entire β-propeller domain of mouse αIIb, attached to the (C-terminal) remainder of the protein from the human αIIb sequence. The human-mouse chimera plasmids are listed in supplemental Table 1 (available on the *Blood* Web site; see the Supplemental Materials link at the top of the online article).

Detection of PA anti-αIIbβ3 Ab binding

αIIb and β3 expression vectors were transiently transfected into 293T cells by lipofection (Lipofectamine2000; Invitrogen). Two days after transfection, the cells were detached from dishes with a solution of 0.02% ethylenediaminetetraacetic acid in PBS (Nakarai tesque); the cells were then washed once with PBS and resuspended at a concentration of 5×10^6/mL in Tyrode buffer with 1mM $CaCl_2$ and 1mM $MgCl_2$. Then, 50-μL aliquots of platelet eluates were incubated with equal amounts of cell suspension for 30 minutes on ice, followed by staining with Alexa Fluor 488–conjugated anti–human IgG (Invitrogen) and phycoerythrin-conjugated anti–human CD61 (Becton Dickinson [BD]). After washing, the cells were resuspended in Tyrode buffer that contained propidium iodine (1 μg/mL) to identify dead cells and then the cells were analyzed on a flow cytometer (FACScan; BD).

PA Ab binding (Alexa 488 staining) was analyzed in a subset of cells that were highly positive for CD61; this subset is denoted by the rectangle (R7) in the dot blots (Figure 1C). We confirmed that $CD61^+$ cells in this region were exclusively complexed with transfected αIIb but not with endogenous α_V by staining with anti-αIIbβ3–specific antibodies; an allophycocyanin (APC)–conjugated anti–human CD41a (clone HIP8; BD), an FITC-conjugated anti–human CD41 (clone P2; Beckman Coulter), and an FITC-conjugated anti–mouse CD41 (clone MWReg30; BD). PA Ab IgG binding 293T cells that expressed chimeric αIIb complexed with human β3 (chimera αIIbβ3) relative to the cells that expressed wild-type human αIIbβ3 (wt αIIbβ3) was calculated as follows: specific PA Ab binding to chimera αIIbβ3/specific PA Ab binding to wt αIIbβ3 × 100 (%).

We always used ≥ 2 eluates obtained from healthy subjects as control in each experiment, and specific IgG binding was calculated by subtracting the mean fluorescence intensity (MFI) of IgG binding in control eluates from the MFI of IgG binding in patient eluates. Expressions of the chimera αIIbβ3 and wt αIIbβ3 cells were monitored by anti-CD61 binding, and the specific PA Ab binding was compensated by CD61 expression.

PA Ab binding to platelets was determined as previously described.[22]

Detection of light chain usage by PA anti-αIIbβ3 Abs

Platelet eluates were incubated with 293T cells that transiently expressed human αIIbβ3. This was followed by incubation with FITC-conjugated anti-κ, PE-conjugated anti-λ Abs (Simultest Anti-Kappa/Anti-Lambda; BD), and APC-conjugated anti-CD61 (Invitrogen). After washing, cells were resuspended in Tyrode buffer that contained propidium iodine. Next, they were analyzed by flow cytometry to evaluate anti-κ and anti-λ Ab binding to cells highly positive for CD61.

Results

Target epitopes of PA anti-αIIbβ3 Abs are mainly localized in the N-terminus of the β-propeller domain in αIIb

We examined PA Ab reactivity to normal platelets and platelets obtained from a patient with type I Glanzmann thrombasthenia (GT), whose platelets completely lack surface αIIbβ3 expression as we previously reported.[23] In eluates from 9 of 10 patients with ITP, the PA Ab reactivity to GT platelets was markedly lower than their reactivity to normal platelets (Figure 2A). The marked reduction in the reactivity to GT platelets was also observed in other 3 eluates (supplemental Figure 1). These results indicated that most PA Abs in these eluates were directed to αIIbβ3. We then examined PA Ab reactivity to 293T cells that expressed mouse αIIbβ3. We found that, in the eluates examined, the PA Abs did not react with mouse αIIbβ3 (Figure 2B). To identify which subunit was essential for the binding, we examined the reactivity to mouse αIIb/human β3 (m2b/H3a) and human αIIb/mouse β3 (H2b/m3a). We found that the PA Abs reacted similarly to cells that expressed H2b/m3a and cells that expressed human αIIbβ3 (38.5%-100%). However, PA Ab reactivity to m2b/H3a was markedly reduced in all 9 eluates examined (1.3%-30.3%; Figure 2C). These results confirmed that the target epitopes of PA anti-αIIbβ3 Abs were mainly present in αIIb.

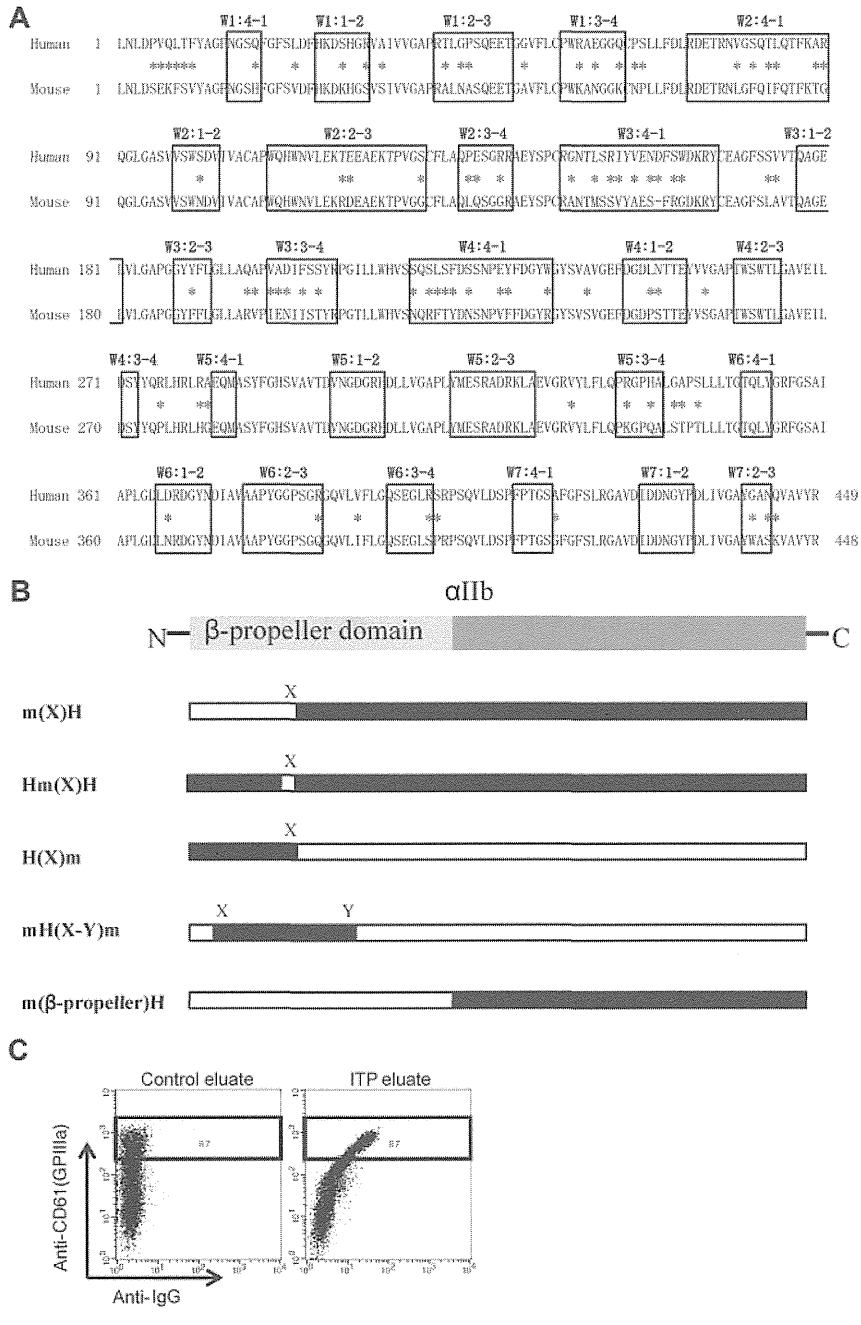

Figure 1. Structure and alignment of the β-propeller domain of αIIb. (A) Human and mouse sequence alignment of the β-propeller domain. The boxes indicate the small loop structures of each β-sheet domain, and the asterisks indicate amino acid difference between human and mouse sequences. (B) Abbreviation of each human-mouse chimeric αIIb/human β3. m(X)H; human αIIb (black) carrying mouse sequences (white) from the N-terminus to the X region. Hm(X)H; human αIIb was exchanged with the only X region for the corresponding sequence of mouse αIIb. H(X)m; mouse αIIb carrying human sequences from the N-terminus to the X region. mH(X-Y)m; mouse αIIb was exchanged with the region of X to Y for the corresponding human αIIb. m(β-propeller)H; human αIIb was exchanged with the entire β-propeller domain of αIIb for the corresponding mouse αIIb. (C) Assessment of PA Abs binding to mutated αIIbβ3-expressing cells. Binding of PA Abs (horizontal) was analyzed in a subset of CD61 highly positive cells denoted by the rectangle (R7) in the dot blots.

We next examined PA anti-αIIbβ3 Ab reactivity with several αIIb chimeras. All αIIb chimeras were expressed with the human β3 on 293T cells. The m(β-propeller)H and m(W4:4-1)H chimeras comprised the human αIIb with substitutions for the mouse β-propeller domain (L1-R449) and the N-terminal half of the β-propeller domain (L1-W235), respectively, because there are few amino acid differences between human and mouse in the C-terminal half of the β-propeller domain (Figure 1B). Compared with wt αIIbβ3, all 15 of the eluates showed markedly impaired binding to cells that expressed the m(β-propeller)H and those that expressed the m(W4:4-1)H chimera (Figure 2D). These results were confirmed by the antigen capture ELISA method in selected patients (supplemental Figure 2). In sharp contrast, most of the 15 eluates tested showed high PA Ab reactivity with the converse αIIb chimeras, H(β-propeller)m and H(W4:4-1)m, complexed with human β3. The PA Ab reactivity was comparable with that observed with wt human αIIbβ3 (Figure 2E). These results indicated that the epitopes of PA anti-αIIbβ3 Abs were mainly localized to the N-terminal half of the β-propeller domain (L1-W235) in αIIb.

Identification of 3 main recognition sites in the N-terminal half of the β-propeller domain in αIIb

Next, we aimed to identify critical target epitopes for PA anti-αIIbβ3 Abs in the N-terminal half of the β-propeller domain in αIIb. For this, we created human-mouse αIIb chimeras that had serial changes in which small sections of human αIIb were exchanged with the corresponding mouse sequences. The series extended from the N-terminus to the W4:4-1 loop (Table 2). We

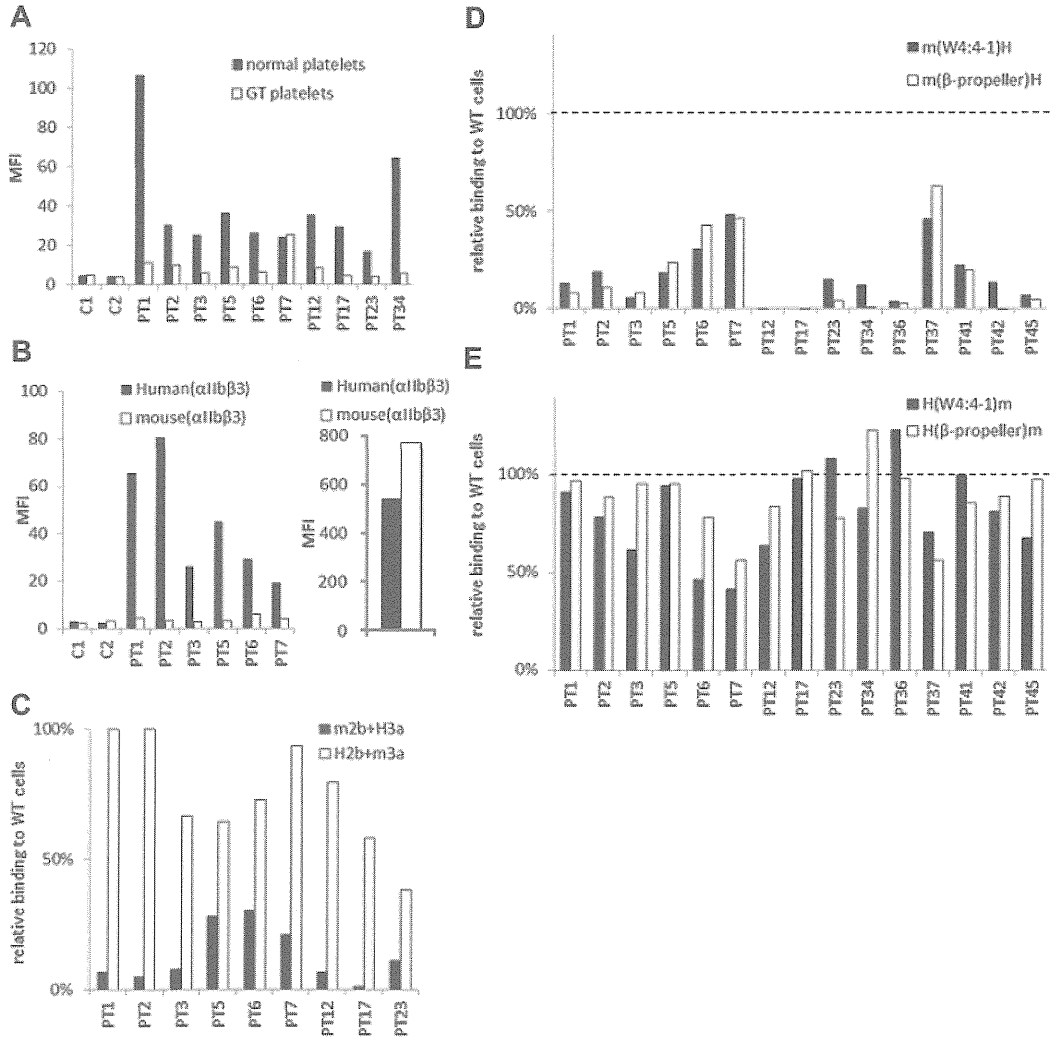

Figure 2. The epitopes of PA anti-αIIbβ3 Abs are mainly localized in the N-terminus of the β-propeller domain of αIIb. (A) Binding of PA Abs to normal (black) or αIIbβ3-deficient platelets (GT platelets; white). C1 and C2 show control eluates. (B) Binding of PA Abs to 293T cells that expressed human (black) or mouse αIIbβ3 (white; left). Expression levels of human and mouse αIIbβ3 were indicated in the right panel monitored by anti-CD61 Ab. (C) Relative binding of PA Abs to 293T cells that expressed mouse αIIb/human β3 (m2b/H3a; black) or human αIIb/mouse β3 (H2b/m3a; white) compared with human αIIbβ3-expressing cells. (D) Relative binding of PA Abs to 293T cells that expressed human αIIb replaced with whole β-propeller domain (white) or the N-terminus to W4:4-1 loop (black) of mouse αIIb with human β3. (E) Relative binding of PA Abs to 293T cells that expressed mouse αIIb replaced with whole β-propeller domain (white) or the N-terminus to W4:4-1 loop (black) of human αIIb with human β3. Shown were means of ≥ 2 independent experiments.

noticed that the reactivity of many PA Abs decreased markedly when a specific loop from human was exchanged for the corresponding mouse sequence. Consequently, we identified 3 groups (A, B, and C) on the basis of loops that appeared to be essential for PA Ab reactivity: the W1:1-2, W1:2-3, and W3:4-1 loops (Table 2). Then, we further characterized the autoantigenic epitopes in each group.

Group A: the W1:1-2 and W2:3-4 loops are essential for PA anti-αIIbβ3Ab binding. In 2 samples (from PTs 17 and 23), the PA Ab reactivity with m(W1:1-2)H, the human αIIb that carried the mouse sequence from the N-terminus to the W1:1-2 loop, was markedly impaired compared with PA Ab reactivity with m(W1:4-1)H (Table 2; Figure 3A). Moreover, these PA Abs showed impaired binding with Hm(W1:1-2)H, the human αIIb that carried only the mouse W1:1-2 loop (Figure 3A). These results suggested that the W1:1-2 loop was essential for PA Ab reactivity in these patients. Conversely, we tested whether we could restore PA Ab reactivity with the mouse αIIb sequence by replacing sections with a series of corresponding human sequences from the N-terminus. We found that PA Ab reactivity in these 2 samples was only restored when the mouse W2:3-4 loop was exchanged with the corresponding human sequence. This was confirmed by the observation that the PA Ab reactivity was markedly impaired for Hm(W2:3-4)H, the human αIIb that carried only the mouse W2:3-4 loop (Figure 3B). These results indicated that both the W1:1-2 and the W2:3-4 loops were essential for PA Ab reactivity. Moreover, the PA Ab reactivity with mH(W1:1-2–W2:3-4)m, the mouse αIIb that carried the human W1:1-2 to W2:3-4 sequence, was not reduced compared with the reactivity with the wt human αIIb. This supported our hypothesis that these PA Abs specifically recognized the W1:1-2 and W2:3-4 loops (Figure 3C).

The W1:1-2 and W2:3-4 loops harbor 2 and 3 amino acid differences between human and mouse, respectively. Therefore, we replaced each of these amino acids in the human sequence with that in the mouse sequence. The S29K and R32S mutations in the W1:1-2 loop and the E136Q and R139G mutations in the W2:3-4 loop almost completely abolished the reactivity of PA Abs from PT 17. The PA Abs from PT 23 also showed markedly impaired reactivity with the R32S and R139G mutations (Figure 3D-E). These results indicated that the S29, R32, E136, and R139 residues in αIIb, particularly the 2 arginines, were critical for the binding of PA Abs in these patients.

Table 2. Percentage of PA Ab binding to human-mouse chimeric αIIbs complexed with human β3 relative to PA Ab binding to wt αIIbβ3 in 293T cells

	m(W1:4-1)H	m(W1:1-2)H	m(W1:2-3)H	m(W2:2-3)H	m(W2:3-4)H	m(W3:4-1)H	m(W4:4-1)H
Group A							
PT 17	99.5*	−1.5*	−1.7	−4.7	NT	−2.9	0.3
PT 23	72.7*	18.9*	−25.0	−18.4	−6.6	−20.6	15.2
Group B							
PT 3	84.4	83.3*	19.6*	12.7	NT	2.9	7.9
PT 36	134.2	116.6*	1.5*	NT	1.7	2.6	3.8
PT 41	88.7	97.5*	50.3*	NT	51.0	44.6	22.3
PT 42	85.6	105.0*	47.5*	NT	41.3	20.5	13.5
PT 12	89.7	87.1	57.5	30.9	9.1	6.8	−1.7
Group C							
PT 1	75.2	NT	93.2	93.7	102.2*	27.3*	13.0
PT 6	109.1	NT	232.2	115.9	103.1*	30.7*	30.7
PT 34	94.0	91.7	108.5	NT	88.3*	−3.4*	12.1
PT 45	94.3	91.4	95.3	NT	73.5*	13.5*	6.5
Others							
PT 2	87.5	80.3	45.8	36.0	NT	19.6	18.9
PT 5	101.5	82.4	74.0	61.6	43.4	39.7	18.3
PT 7	104.9	NT	111.4	90.5	105.3	60.3	48.6
PT 37	123.5	128.5	102.8	NT	114.1	65.4	45.9

The PT no. designates the ITP sample that was tested for binding to cells that expressed the indicated chimeras. Values are percentages and represent the means of ≥ 2 independent experiments.

NT indicates not tested.

*Marked reductions (> 40%) in binding between 2 loops in addition to marked reduction (> 40%) in binding compared with binding with wt αIIbβ3.

Group B: the W1:2-3 loop is essential for PA anti-αIIbβ3Ab binding. In 5 samples (from PTs 3, 12, 36, 41, and 42), the PA Ab reactivity was impaired with m(W1:2-3)H compared with m(W1:1-2)H (Table 2; Figure 4A). The sample from PT 36 showed complete loss of PA Ab reactivity with m(W1:2-3)H. The reactivity with Hm(W1:2-3)H was essentially the same as the reactivity with

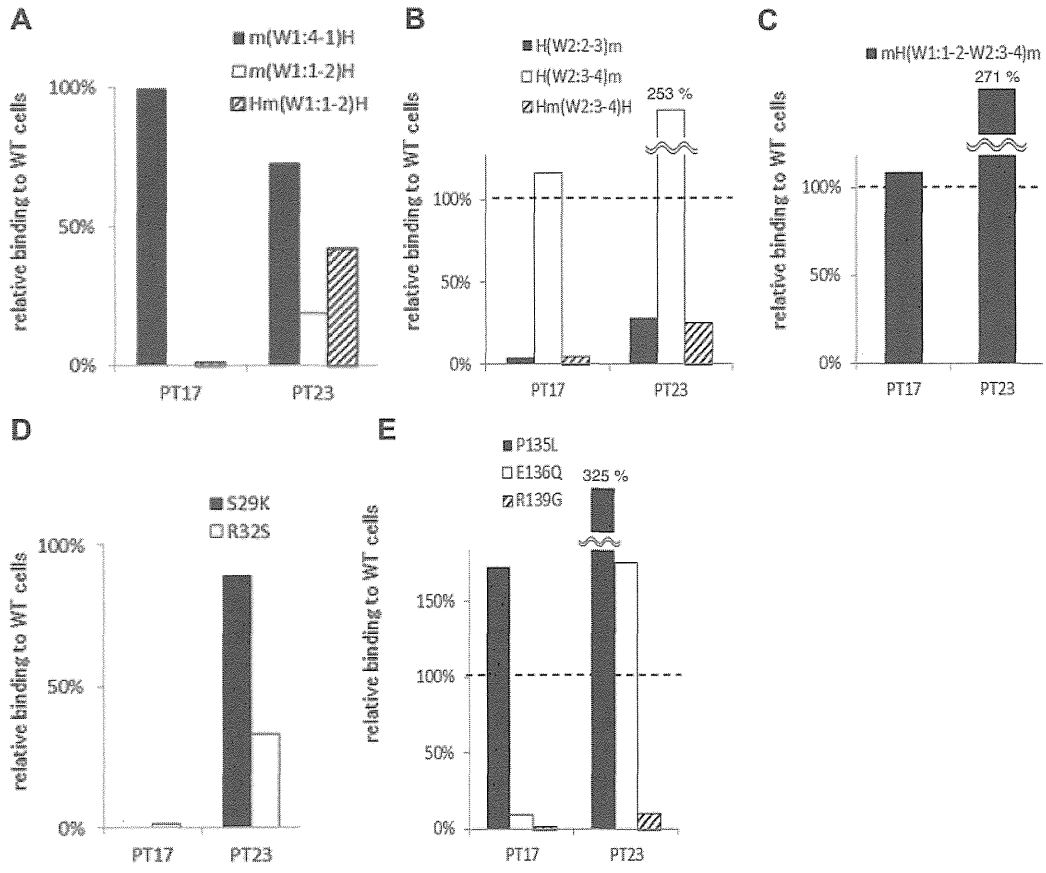

Figure 3. Group A: the W1:1-2 and W2:3-4 loops are essential for PA anti-αIIbβ3 Ab binding. (A) Relative binding of PA Abs in 2 patients (PTs 17 and 23) to m(W1:4-1)H (black), m(W1:1-2)H (white), and Hm(W1:1-2)H (shaded) compared with wt αIIbβ3. (B) Relative binding of PA Abs to H(W2:2-3)m (black), H(W2:3-4)m (white), and Hm(W2:3-4)H (shaded). (C) Relative binding of PA Abs to mH(W1:1-2–W2:3-4)m that the mouse αIIb carried the human W1:1-2 to W2:3-4 sequences. (D) Relative binding of PA Abs to S29K (black) and R32S (white) mutants. (E) Relative binding of PA Abs to P135L (black), E136Q (white) and R139G (shaded) mutants. Shown were means of ≥ 2 independent experiments.

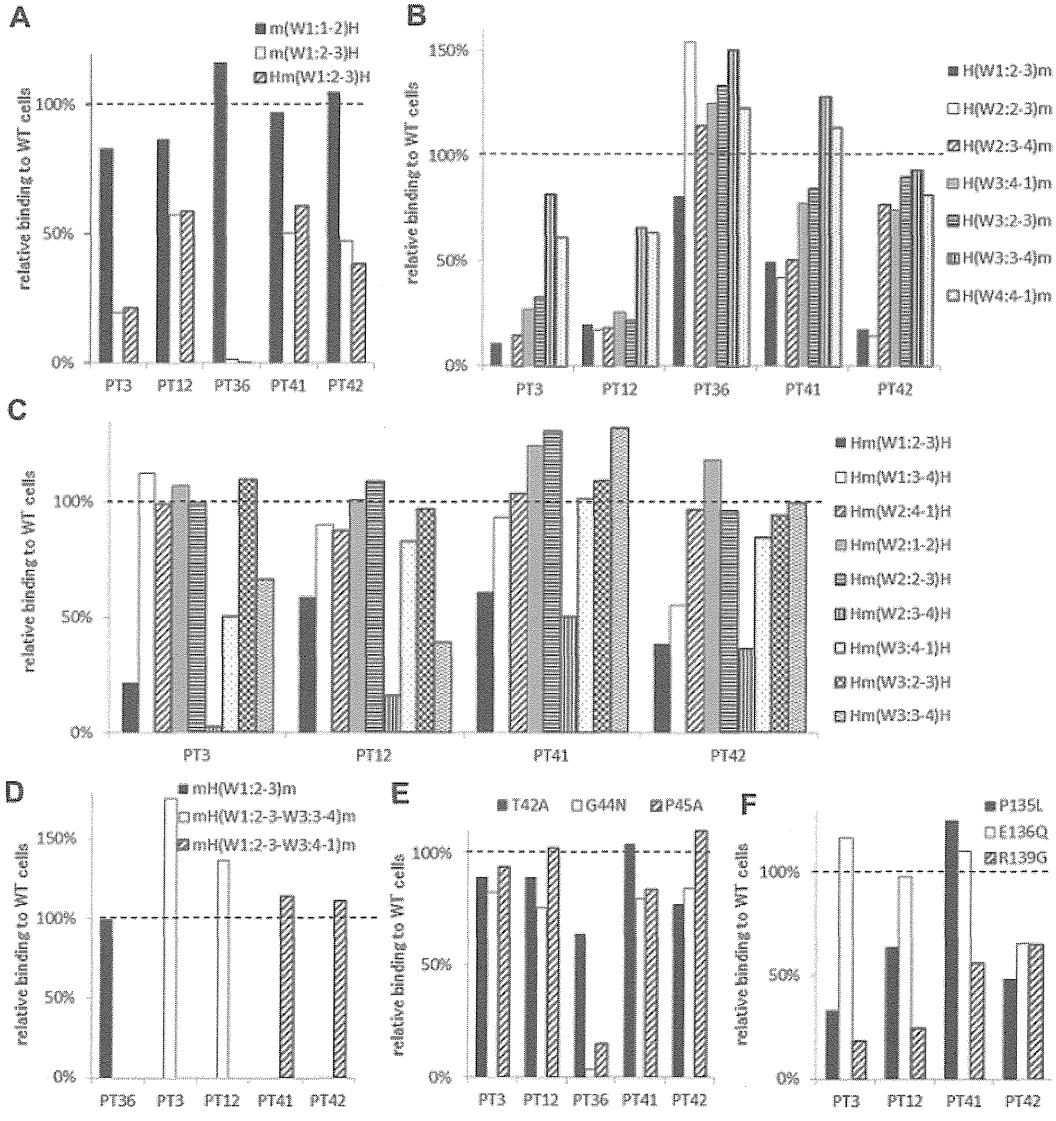

Figure 4. Group B: the W1:2-3 loop is essential for PA anti-αIIbβ3 Ab binding. (A) Relative binding of PA Abs in 5 patients (PTs 3, 12, 36, 41 and 42) to m(W1:1-2)H (black), m(W1:2-3)H (white), and Hm(W1:2-3)H (shaded) compared with wt αIIbβ3. (B) Relative binding of PA Abs to mouse αIIb replaced from the N-terminus to the indicated loops with the corresponding human sequences. (C) Relative binding of PA Abs to human αIIb replaced the indicated loop with the corresponding mouse sequences. (D) Relative binding of PA Abs to mH(W1:2-3)m (black), mH(W1:2-3–W3:3-4)m (white), and mH(W1:2-3–W3:4-1)m (shaded). (E) Relative binding of PA Abs to T42A (black), G44N (white), and P45A (shaded) mutants. (F) Relative binding of PA Abs to P135L (black), E136G (white), and R139G (shaded) mutants. Shown were means of ≥ 2 independent experiments.

m(W1:2-3)H (Figure 4A). These results suggested that the W1:2-3 loop was essential for PA Ab reactivity in these samples. Again, we tested whether we could restore PA Ab reactivity with the mouse αIIb sequence by replacing sections with a series of corresponding human sequences from the N-terminus (Figure 4B). We found that the PA Ab reactivity in the sample from PT 36 was almost fully restored with H(W1:2-3)m, which had the human amino acid sequence from the N-terminus to the W1:2-3 loop. The sample reactivity from PT 36 with mH(W1:2-3)m was the same as that observed with the wt human αIIbβ3 sequence (Figure 4D). These results suggested that the W1:2-3 loop contained an epitope(s) for PA anti-αIIbβ3 Abs in the sample from PT 36.

In contrast, the PA Abs in the samples from PTs 3 and 12 showed restored reactivities with H(W3:3-4)m, and the samples from PT 41 and PT 42 showed restored reactivities with H(W3:4-1)m and H(W2:3-4)m, respectively (Figure 4B). These results suggested that loop(s) other than the W1:2-3 may be important for PA Ab reactivity in these patients. To localize the epitope(s) important for PA Ab reactivity in these patients, we constructed human αIIb expression vectors in which each surface loop from W1:2-3 to W3:3-4 was replaced with the corresponding mouse sequence (Figure 4C). We found that the PA Abs from these 4 patients showed impaired reactivity with Hm(W1:2-3)H and Hm(W2:3-4)H. This indicated that both the W1:2-3 and the W2:3-4 loops were involved in PA Ab binding efficiency. In addition, the W3:3-4 loop also appeared to be involved in PA Ab reactivity in samples from PTs 3 and 12 (Figure 4C). Furthermore, PA Ab binding was fully restored to levels observed with wt αIIb, when the samples from PTs 3 and 12 reacted with mH(W1:2-3-W3:3-4)m and the samples from PTs 41 and 42 reacted with mH(W1:2-3-W3:4-1)m (Figure 4D). These results suggested that the PA Abs from PTs 3 and 12 mainly recognized the W1:2-3, W2:3-4, and W3:3-4 loops and that the PA Abs from PTs 41 and 42 recognized the W1:2-3 and W2:3-4 loops.

There are 3 amino acid differences between human and mouse in each W1:2-3 and W2:3-4 loop. These are the T42A, G44N, and P45A in the W1:2-3 loop and P135L, E136Q, and R139G in the